

RESEARCH ARTICLE

10.1002/2017JB015112

Special Section:

Ten years after the Wenchuan earthquake: new insights into the geodynamics of the eastern Tibet

Key Points:

- New paleomagnetic results on Middle Jurassic and Paleocene rocks suggest that northern Sibumasu underwent a $\sim 80^\circ$ CW rotation
- Eastward motion of Tibetan crustal material along the Xianshuihe-Xiaojiang fault after Middle Miocene is transmitted toward Myanmar
- The orientation of Qiangtang/Sibumasu is $N60^\circ W$ in Tibet and $N10^\circ W$ in southern Sibumasu

Supporting Information:

- Supporting Information S1

Correspondence to:

S. Li and C. Deng,
lsh917@mail.iggcas.ac.cn;
lishihu@mail.sysu.edu.cn;
cldeng@mail.iggcas.ac.cn

Citation:

Li, S., van Hinsbergen, D. J. J., Deng, C., Advokaat, E. L., & Zhu, R. (2018). Paleomagnetic constraints from the Baoshan area on the deformation of the Qiangtang-Sibumasu terrane around the eastern Himalayan syntaxis. *Journal of Geophysical Research: Solid Earth*, 123, 977–997. <https://doi.org/10.1002/2017JB015112>

Received 13 OCT 2017

Accepted 22 JAN 2018

Accepted article online 25 JAN 2018

Published online 12 FEB 2018

Paleomagnetic Constraints From the Baoshan Area on the Deformation of the Qiangtang-Sibumasu Terrane Around the Eastern Himalayan Syntaxis

Shihu Li^{1,2} , Douwe J. J. van Hinsbergen³ , Chenglong Deng² , Eldert L. Advokaat³, and Rixiang Zhu² 

¹Guangdong Provincial Key Laboratory of Geodynamics and Geohazards, School of Earth Sciences and Engineering, Sun Yat-sen University, Guangzhou, China, ²State Key Laboratory of Lithospheric Evolution, Institute of Geology and Geophysics, Chinese Academy of Sciences, Beijing, China, ³Department of Earth Sciences, Utrecht University, Utrecht, The Netherlands

Abstract The Sibumasu Block in SE Asia represents the eastward continuation of the Qiangtang Block. Here we report a detailed rock magnetic and paleomagnetic study on the Middle Jurassic and Paleocene rocks from northern Sibumasu, to document the crustal deformation during the India-Asia collision since the Paleocene and reconstruct the overall strike of the Qiangtang/Sibumasu elements before the India-Asia collision. Although the fold test is inconclusive based solely on our data, a positive reversal test, a positive regional fold test with previous paleomagnetic results, and a detrital origin of hematite in the red beds as indicated by scanning electron microscopy suggest that the magnetizations obtained from the Jurassic and Paleocene rocks are most likely primary, showing an $\sim 80^\circ$ clockwise rotation since Paleocene. These results, together with previously published paleomagnetic data, suggest that the northern Sibumasu and northern Simao elements experienced a $\sim 60\text{--}80^\circ$ clockwise rotation since Paleocene. This large clockwise rotation is also consistent with the surface GPS velocity field and NE-SW fault networks, suggesting a rotational motion of crustal material from southeastern Tibet during late Cenozoic. We infer that the large clockwise rotation is a sum of rotation in the Eocene to Middle Miocene time associated with Indochina extrusion and rotation after the Middle Miocene associated with the E-W extension in central Tibet. This suggests that the eastward motion of Tibetan crustal material along the Xianshuihe-Xiaojiang fault after Middle Miocene is transmitted to the southwest toward Myanmar. Jurassic and Cretaceous paleomagnetic results suggest that the Qiangtang/northern Sibumasu was originally a curved structure with an orientation of $N60^\circ W$ in Tibet and changes to $N10^\circ W$ in southern Sibumasu.

1. Introduction

When the continental crust of Indian plate collided with Eurasia, a collage of pre-existing terranes in the Tibetan Plateau and Indochina became intensely deformed by shortening, strike-slip faulting, and vertical axis rotations. Restoring this collage into its precollisional configuration is then key to deducing the dynamics of the crustal and lithospheric response to collision. In this paper, we contribute to this reconstruction by providing new paleomagnetic data in an intensely deformed region in the southeast margin of the collision zone.

The Tibetan and SE Asian tectonic collage consists of Gondwana-derived continental fragments separated by Paleozoic to Cenozoic sutures where oceanic basins were consumed. These include the blocks of South China, Indochina, Sibumasu-Qiangtang, Lhasa, and West Burma (e.g., Metcalfe, 2013), whereby the latter may (Liu et al., 2016) or may not (Sevastjanova et al., 2016) have once formed one contiguous terrane (Figure 1). These terranes were separated from Gondwana, drifted to the north, and eventually accreted to North China and Siberia throughout the Paleozoic and Mesozoic, associated with the opening and subduction of Tethyan Ocean System: the Paleo-Tethys Ocean from the Devonian to Triassic, the Meso-Tethys Ocean from the late Early Permian to Late Cretaceous, and the Neo-Tethys Ocean from the Late Triassic to Late Cretaceous (e.g., Li et al., 2016; Metcalfe, 2013; Song et al., 2017). The Paleo-Tethys suture represents the collision of Qiangtang/Sibumasu with South China in the Early to Late Triassic, it is exposed along the Jinshajiang belt in central Tibet (Wang et al., 2000), the Changning-Menglian belt in southwest China, and the Bentong-Raub suture in Thailand and Malaysia (Metcalfe, 1996, Figure 1). The Meso-Tethys suture represents the collision of Lhasa, West Burma with Qiangtang/Sibumasu in Early to mid-Cretaceous, is exposed

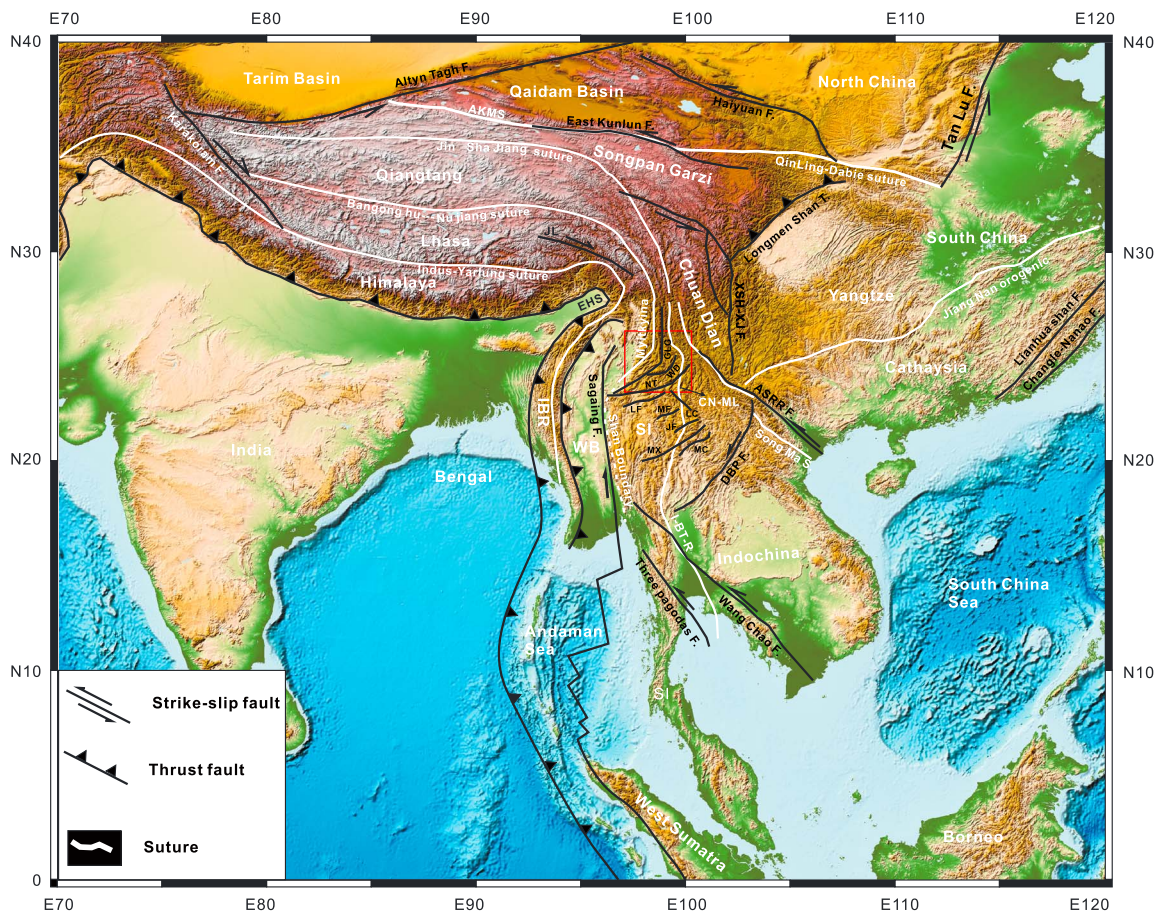


Figure 1. Outline tectonic map of the SE Asia. AKMS: Anyimaqin-Kunlun-Muztagh suture; ASRRF: Ailao Shan-Red River fault; CN-ML: Changning-Menglian suture zone; DBPF: Dien Bien Phu fault; EHS: Eastern Himalaya syntaxis; GLG: Gaoligong shear zone; IBR: Indo-Burma Ranges; I-BT-R: Inthanon-Bentong-Raub suture; JF: Jinghong fault; JL: Jialili fault; LC: Lincang fault; LF: Lashio fault; MC: Mae Chan fault; MF: Menglian fault; MX: Mengxing fault; NT: Nanting river fault; SI: Sibumasu Block; WD: Wandering fault; XSH-XJF: Xianshuihe-Xiaojiang fault. The red square denotes the location of Figure 2.

along the Bangong-Nujiang suture in central Tibet, and continues southeastward to the Myitkyina suture in eastern Myanmar (Liu et al., 2016, Figure 1). The Neo-Tethys suture is the locality where the initial India-Asia collision happened; it includes the Yarlung-Tsangpo suture in southern Tibet and the Kalaymyo suture in the Indo-Burman Ranges (Liu et al., 2016, Figure 1).

Reconstructing the original orientations of these sutures, and hence the contiguity and orientations upon collision of the adjacent continental blocks, is hampered by the intense deformation that occurred after their collision and accretion, in particular, since the Cenozoic India-Asia collision. In Late Cretaceous and especially Cenozoic time, the southeast margin of Tibetan Plateau experienced major deformation, in the form of crustal shortening, strike-slip faulting, and vertical axis rotations (e.g., Leloup et al., 1995; Li, Yang, et al., 2017; Li, Advokaat, et al., 2017; Wang et al., 1998; Yang et al., 1995, 2001; Zhang et al., 2004). Kinematically restoring these deformation processes provides important constraints on the tectonic evolution of Tibetan Plateau and is key to reconstructing the paleogeography of the Tethys oceans.

Based on suture ages and correlations of continental rock assemblages, the Bangong-Nujiang suture between the Qiangtang/Sibumasu and Lhasa terranes was mapped to curve around the eastern Himalayan syntaxis, making an angle of as much as 150°. Current retrodeformations of the larger Indochina Block aimed to restore motions on major faults in Yunnan and Indochina. These restorations restored from as little as 250 km (e.g., Hall, 2002; van Hinsbergen et al., 2011) to as much as 1,000 km or more (e.g., Royden et al., 2008) of Indochina extrusion in Cenozoic time, associated with ~10–40° of clockwise rotation. Based on these reconstructions, the Lhasa terrane would have had a sharp paleogeographic kink along its eastern margin. A recent compilation of paleomagnetic data showed that the Indochina Block may be

divided into several quasi-rigid terranes, that is, terranes that underwent a similar vertical axis rotation but that were likely internally shortened (Li, Advokaat, et al., 2017). This compilation suggested that northwestern Indochina experienced much larger rotations than the main, SE part of Indochina. Restoring these rotations suggested that NW Indochina may have been extruded by at least 350 km more than SE Indochina in the Cenozoic, reconciling large (~600 km in the NW) and small (~250 km in the SE) estimates of extrusion of the Indochina Block. However, paleomagnetic data from the Qiangtang and Sibumasu Blocks adjacent to the strongly curved Bangong-Nujiang suture south of the eastern Himalayan syntaxis are scarce, and this suture remains essentially unreconstructed into any form of pre-Cenozoic orientation.

In this paper, we present a detailed paleomagnetic study of Jurassic and Paleocene sedimentary rocks from the northern Sibumasu Block adjacent to the Bangong-Nujiang suture in the Baoshan area, in an attempt to quantify the rotation accumulated since the Cretaceous. Based on these results, we discuss the kinematic evolution of the western Yunnan area and reconstruct the paleogeography of Qiangtang/Sibumasu before India-Asia collision. In combination with GPS data and recent fault displacements, we also discuss the implications of our findings for how Miocene to recent crustal motions around the eastern Himalayan syntaxis have been accommodated.

2. Geologic Setting and Sampling

The N-S trending Sibumasu Block is separated from the Indochina Block by the Changning-Menglian-Chiang Mai-Inthanon suture zone to the east and from the West Burma Block by the Myitkyina suture to the west (Metcalf, 2013; Figure 1). The Indochina Block is further separated from the South China Block by the Jinshajiang-Majiang suture, while the West Burma Block is separated from the Indo-Burma Ranges by the Kalaymyo suture (Figure 1). In central Tibet, the Qiangtang Block is separated from the Songpan-Garzi Block by the Jinshajiang suture to the north and separated from the Lhasa Block by the Bangong-Nujiang suture to the south (Figure 1). South of the Lhasa Block lies the Tethy Himalaya that is bounded by the Indos-Yarlung suture (Figure 1). Based on suture ages and correlations of continental rock assemblages, the Jinshajiang suture has been suggested to connect to the Changning-Menglian-Chiang Mai-Inthanon suture, the Bangong-Nujiang suture connects to the Myitkyina suture and may extend further south to connect the Shan boundary, and the Indos-Yarlung suture connects to the Kalaymyo suture (Liu et al., 2016; Metcalf, 1996, 2013; Mitchell et al., 2015; Zhai et al., 2013, Figure 1). Therefore, the Sibumasu Block represents the eastward extension of Qiangtang Block. The West Burma Block may represent the eastern continuation of Lhasa element (Figure 1).

These main basement curved elements and intervening sutures of the Yunnan area have been deformed by major Cenozoic strike-slip fault systems (Leloup et al., 1995; Tapponnier et al., 1982), the most prominent of which include the Sagaing fault, the Gaoligong shear zone, the Chongshan shear zone, the Ailao Shan-Red River shear zone, and the Xianshuihe-Xiaojiang fault (Figure 1). The Ailao Shan-Red River shear zone is regarded as the eastern boundary fault that accommodated large magnitude southeastward extrusion of the Indochina Block (Leloup et al., 1995; Tapponnier et al., 1982) between 35 and 17 Ma (Gilley, 2003; Leloup et al., 1995, 2001) or during a shorter time window in this interval (Searle et al., 2010). Estimates of the amount of extrusion vary strongly along-strike, with estimates of 700 ± 200 km based on markers in the northwest of the fault (Chung et al., 1997; Leloup et al., 1995, 2001) but no more than ~250 km based on observations along the southeastern part of the fault (Fyhn et al., 2009; Mazur et al., 2012; Wang & Burchfiel, 1997). Li, Advokaat, et al. (2017) recently noted that these estimates may be reconciled by restoring paleomagnetically documented vertical axis rotations of fault-bounded blocks in NW Indochina, such that early Eocene extrusion of some 350 km was accommodated by rotation and deformation within NW Indochina, and later extrusion in the Oligocene-early Miocene led to an additional 250 km of extrusion of the whole of Indochina. The Red River fault inverted as a dextral fault since the late Miocene (Leloup et al., 1993; Li et al., 2013; Schoenbohm, Burchfiel, Chen, Yin, 2006) and accommodated a ~40 km right-lateral strike-slip displacement (Schoenbohm, Burchfiel, Chen, Yin, 2006; Wang et al., 1998).

The left-lateral Xianshuihe-Xiaojiang fault is regarded as a boundary fault to accommodate the eastward motion of Tibetan crustal materials around the eastern Himalayan syntaxis (Schoenbohm, Burchfiel, & Chen, 2006; Wang et al., 1998, Figure 1) that is still active, as well as imaged by GPS measurements (Zhang et al., 2004). The Xianshuihe-Xiaojiang fault initiated at ca. 13 Ma (Li et al., 2015; Roger et al., 1995; Wang

et al., 2009) and has accumulated a total displacement of ~80–100 km (Wang et al., 1998). It is kinematically linked to E-W extension that has affected the Tibetan Plateau since middle Miocene time (e.g., Blisniuk et al., 2001). Eastward crustal transfer (thought to be driven by lower crustal flow; e.g., Clark & Royden, 2000) is in eastern Tibet associated with E-W shortening and uplift of the Longmen Shan (e.g., Kirby et al., 2002), whereas to the south, crust is transferred toward the Yunnan area along the Xianshuihe-Xiaojiang fault. This fault terminates to the south before reaching the Ailao Shan-Red River shear zone. How and where the southward motion of crust along the Xianshuihe-Xiaojiang fault is accommodated in the southwestern Yunnan area remain poorly determined. Southwest of the Ailao Shan-Red River shear zone, a set of strongly curved, NE–SW striking, sinistral strike-slip faults is present, such as the Wanding, Nanting river, Mengxing, Dien Bien Phu faults (Lacassin et al., 1998; Socquet & Pubellier, 2005; Wang & Burchfiel, 1997; Wang et al., 1998, Figure 1), which may transfer (some of) the Miocene motion along the Xianshuihe-Xiaojiang fault toward the Burma trench and the fold-thrust belt of the outer Burman ranges that form the plate boundary with India (e.g., Gahalaut et al., 2013; Maurin & Rangin, 2009). Recently, Wang et al. (2014) carried out a systematic field study on these NE–SW faults. Based on the geomorphology, river offset across the faults, and fault bounded basins, most of these faults are suggested to be left lateral, active at least in late Miocene, and the left-lateral displacement is estimated to be ~4 km along Dayingjiang fault, ~11 km along Ruili fault, ~10 km along Wanding fault, ~21 km along Nanting river fault, ~24 km along Mengxing fault, ~11 km along Jinghong fault, ~5.5 km along Lashio fault, ~4 km along Mae Chan fault, and ~12.5 km along Dien Bien Phu fault (Figure 1), which suggests a total displacement of ~90 km. Some of the rivers show hairpin geometries when crossing these active strike-slip faults, which may suggest a regional reversal of slip sense from right to left lateral sometime between 5 and 20 Ma (Lacassin et al., 1998).

The ductile right-lateral Gaoligong shear zone and the Shan Scarp are regarded as the western boundary of the extruding Indochina-Sibumasu domain during the Cenozoic prior to the activity of the Sagaing fault (Akciz et al., 2008; van Hinsbergen et al., 2011; Wang et al., 2006, Figure 1). This fault system strikes N-S in the north, changes abruptly to NE–SW and E-W in the Mogok belt where it was associated with N-S extension and exhumation (Searle et al., 2007), and curves back to N-S striking along the Shan Scarp. Geochronologic data suggest that the strike-slip shearing along the Gaoligong shear zone and Shan Scarp occurred in Oligocene to middle Miocene time (Bertrand et al., 2001; Searle et al., 2007, 2010; Wang et al., 2006; Zhang et al., 2012), contemporaneous with the left-lateral strike-slip on the Ailao Shan-Red River shear zone. To the west of the Gaoligong shear zone lies the Sagaing fault, which accommodates parts of the northward motion of India plate. The Sagaing fault is a dextral strike-slip fault initiated at ca. 11 Ma, with a total displacement of ~500 km. In the south, the fault is linked to the ridge of the Andaman Sea (Curry, 2005, Figure 1).

To the north of the Sibumasu Block lies the Baoshan and Tengchong area (Figure 1). The Baoshan area is defined as the triangular area north of the Nanting river fault, east of Gaoligong fault, and west of Chongshan fault. The Tengchong area is bounded between the Myitkyina suture and Gaoligong fault (Figure 2). The Baoshan area consists mostly of platform carbonate rocks and detrital sediments with ages ranging from Late Cambrian to Jurassic. Minor volcanic rocks are exposed in some intervals in the Lower Permian, Upper Triassic, Middle Jurassic, and Cenozoic (Yunnan Bureau of Geology and Mineral Resources (YBGMR), 1990). Two red bed formations suggesting the presence of hematite are particularly well suited for paleomagnetic research. The oldest of these is the Luzijiang Formation, and it unconformably overlies Upper Triassic strata and mainly consists of purple red mudstones, sandstones, and conglomerates. It has a thickness of ~800 m and is mainly exposed around the Yongde County (Figure 2). The presence of *Cuneopsis* spp. bivalvia and *Burmihynchia praestans* brachiopods suggests a Middle Jurassic age (J2l) of the Luzijiang Formation (YBGMR, 1990). The younger sequence is the Paleocene Muguaha Formation (E1g), and this unconformably overlies Paleozoic and Mesozoic strata and is conformably overlain by coarse sandstones and conglomerates of the Eocene-Oligocene Zhushan Formation (E2z). The Muguaha Formation mainly consists of hematitic sandstones and mudstones with a thickness of ~750 m. The presence of charophyte flora fossils (e.g., *Obtusochara lanpingensis*, *Tectochara subelongta*, and *Rhabdochara* sp.) and ostracoda fossils (e.g., *Sinocypris menglaensis*, *S. jinghongensis*, *S. cf. favosa*, and *S. reniformis*) indicates an early to middle Paleocene age of the Muguaha Formation (YBGMR, 1990; Tong et al., 2016). Neogene sediments are rare and mainly consist of upper Pliocene coal-bearing clay and unconsolidated Quaternary conglomerates.

Paleomagnetic samples were collected from the Jurassic Luzijiang Formation and Paleocene Muguaha Formation north of the Yongde County (Figure 2). In each formation, 10 sites (distinct beds) were sampled,

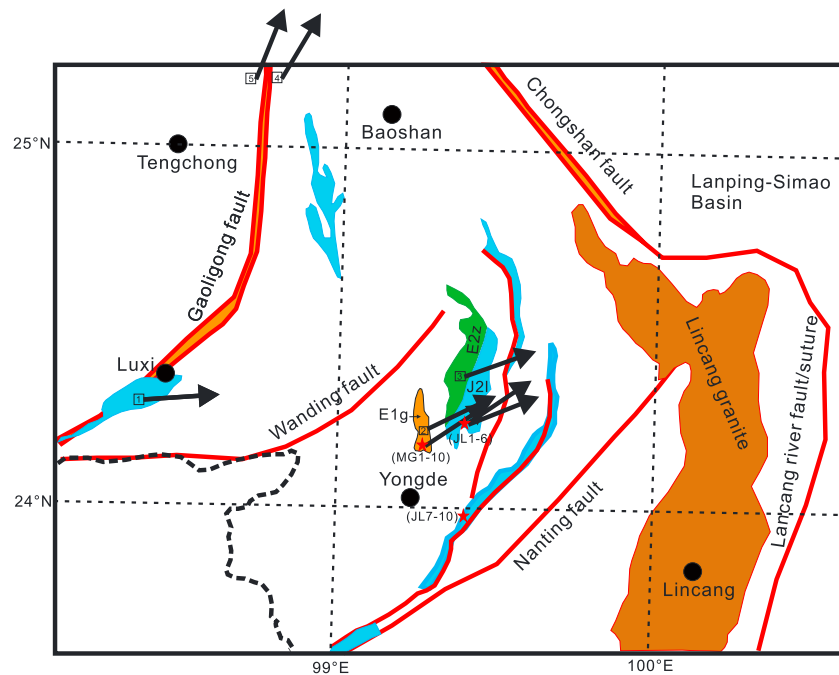


Figure 2. Simplified geological map of the Baoshan area. The black arrows denote the paleomagnetic directions. The red star represents the location of this study. Numbers in square represent previous studies. 1: Huang and Opdyke (1993); 2 and 3: Tong et al. (2016); 4: Kornfeld, Eckert, Appel, Ratschbacher, Pfander, et al. (2014); 5: Kornfeld, Eckert, Appel, Ratschbacher, Sonntag, et al. (2014). J2l: Middle Jurassic Luzijing Formation; E1g: Paleocene Muguahae Formation; E2z: Oligocene Zhushan Formation.

and each site contains 9–18 independent samples. A gasoline-powered drill was used to take the core of 2.5 cm in diameter, which were then oriented with a magnetic compass in the field. In total, 255 samples (114 from the Jurassic Luzijing Formation and 141 from the Paleocene Muguahae Formation) were collected, and all the samples were cut into one to two standard cylinder paleomagnetic specimens of 2.2 cm in height in the laboratory.

3. Methods

3.1. Rock Magnetic Measurements

In order to determine the key magnetic remanence carriers in the Jurassic Luzijing Formation and Paleocene Muguahae Formation, systematic rock magnetic measurements were conducted on four representative samples (two from each formation), which include three-axis isothermal remanent magnetization (IRM), hysteresis loops, IRM acquisition curves, and DC field demagnetization of the saturation IRM (SIRM). To acquire the Lowrie three-axis IRM, the samples were first magnetized in DC fields of 1.5 T, 0.5 T, and 0.15 T along three mutually orthogonal axes using a 2G Enterprises Pulse Magnetizer (2G660; Lowrie, 1990) and then thermally demagnetized progressively up to 685°C with intervals of 10–50°C using a thermal demagnetizer (ASC TD-48). Hysteresis loops were performed with an alternating gradient force magnetometer (VSM 3900). For each sample the magnetic field was cycled with a maximum field of 1.5 T. Saturation magnetization (M_s), saturation remanence (M_{rs}), and coercivity (B_c) were calculated after subtracting the paramagnetic contributions. The IRM acquisition curve was also measured by VSM 3900 by applying a field from 0 to 1.5 T. The remanence coercivity (B_{cr}) was obtained by stepwise demagnetization of SIRM in a backfield up to -1.0 T. All the paleomagnetic and mineral magnetic experiments were measured in the Paleomagnetism and Geochronology Laboratory, Institute of Geology and Geophysics, Chinese Academy of Science (IGGCAS).

3.2. Scanning Electron Microscope Observations

To better constrain the microtexture and origin of the magnetic minerals, polished thin sections of four samples from the Jurassic Luzijing and Paleocene Muguahae Formations were studied using a scanning

electron microscope (SEM; FEI Nova NanoSEM 450) with an energy dispersive spectrometer (EDS; Oxford X-MAX80) at the State Key Laboratory of Lithospheric Evolution, IGGCAS. EDS analysis was subsequently conducted to obtain compositional information.

3.3. Demagnetization of the Natural Remanent Magnetization

All samples were subjected to stepwise thermal demagnetization up to 690°C using an ASC TD-48 thermal demagnetizer. The temperature interval is 25–50°C below 585°C and is 10–15°C above 585°C. Remanence was measured using a 2G Enterprises Model 755 cryogenic magnetometer, which was situated in a magnetically shielded room (<300 nT). The principal component analysis was computed either by least-squares fits (Kirschvink, 1980) or by the great circle path (McFadden & McElhinny, 1988). The online tool set Paleomagnetism.org (Koymans et al., 2016) and Pmagpy software (Tauxe, 2010) were employed to analyze the data.

Traditionally, paleomagnetic directions were obtained by using Fisher statistics (Fisher, 1953) to average a few site mean directions, which were derived from averaging a few specimens within each site. However, as described in Deenen et al. (2011), Fisher statistics is only an appropriate approximation of paleomagnetic distributions when applied on virtual geomagnetic pole (VGP) distributions instead of directions. Therefore, the mean directions were computed using Fisher statistics (Fisher, 1953) on VGPs where each sample represents an independent direction and the observed scatter is resulted from paleosecular variation (PSV). An error in declination ΔD_x and an error in inclination ΔI_x were calculated following Butler (1992) and Deenen et al. (2011). We applied a fixed 45° cutoff (Biggin et al., 2008; Johnson et al., 2008) and applied the n -dependent reliability envelope $A_{95\min, \max}$ of Deenen et al. (2011) to test whether the VGP scatter of site distributions may be straightforwardly explained by PSV. Sites with an A_{95} larger than $A_{95\max}$ must contain extra sources of scatter (e.g., through differential block rotations), while sites with $A_{95} < A_{95\min}$ underrepresent PSV (e.g., as a result of remagnetization), and their validity needs to be discussed. Because we use these criteria to test whether PSV is accurately represented in the data and to weigh sites against the degree to which they average PSV, our locality averages are based on averaging all individual sample directions of the locality, following Deenen et al. (2011). The classical approach in paleomagnetism is to average the individual site mean directions instead, and for illustration, averages of site averages are also provided in Table 1. The differences between the two approaches are statistically insignificant. In addition, we have performed where possible fold tests (Tauxe & Watson, 1994) and reversal tests (McFadden & McElhinny, 1990; Tauxe, 2010).

4. Results

4.1. Rock Magnetic Results

Thermal demagnetization curves of the three-component IRM show that the intensity of all the three components decrease quickly above 650°C and unblock up to 680°C (Figure 3), suggesting the dominance of high-coercivity hematite. This is confirmed by the hysteresis loops and IRM acquisition curves. The hysteresis loops are closed until the maximum field of 1.5 T (Figures 4a–4d), and the magnetic remanence of IRM acquisition curves is still not saturated at the maximum applied field of 1.5 T (Figures 4e–4h). All of these results indicate that hematite is the main magnetic remanence carrier in the sediments. However, we noticed that in some specimens (e.g., MG4-2), minor low coercivity magnetic minerals (e.g., magnetite) may also be present as the hysteresis loop shows a weak wasp waist character (Roberts et al., 1995; Figure 4d). The IRM component analyses show a single high-coercivity component, which confirms the dominance of hematite (Figures 4i–4l).

4.2. Petrography Results

Based on the rock magnetic results and EDS analysis, we know that hematite is the main magnetic mineral in the Jurassic Luzijing and Paleocene Muguahé Formations. However, the morphologies of hematite show two different behaviors within different specimens (Figure 5). The first type of specimens, including one from the Luzijing Formation (Figures 5a–5c) and two from the Muguahé Formation (Figures 5g–5i), shows rectangle, triangle, subrounded, or irregular shape of the hematite, with a grain size of tens of micrometers, suggesting a detrital origin. The second type, from one specimen (JL7–6) of the Jurassic Luzijing Formation, shows that most hematite are distributed either along cracks and pores or around edges of quartz and feldspar grains

Table 1
Paleomagnetic Data From the Middle Jurassic Luzijiang Formation (J2) and Paleocene Muguahue Formation (E1m) From Baoshan, Northern Sibumasu

Site	Locality			In situ										Tilt-corrected					Method		
	Age	Lat (°N)	Long (°E)	Bedding dip/dip(°)	n/n ₀	D _g (°)	ΔD _x (°)	I _g (°)	ΔI _x (°)	K	A ₉₅	D _s (°)	ΔD _x (°)	I _s (°)	ΔI _x (°)	K	A ₉₅	A _{95min}		A _{95max}	
																					Age
Middle Jurassic Luzijiang Formation																					
JL1	J2	24.3	99.6	143/44	12/12	221.1	4.5	-35.0	6.4	106.2	4.4	252.2	4.3	-31.9	6.6	110.3	4.2	4.4	17.1	GC	
JL2	J2	24.3	99.6	140/41	12/12	366	3.0	50.3	2.9	277.1	2.6	82.3	2.7	42.6	3.2	315.8	2.4	4.4	17.1	PCA	
JL3	J2	24.3	99.6	141/45	11/11	34.3	2.5	40.2	3.2	388.5	2.3	68.4	2.9	31.3	4.4	277.8	2.7	4.6	18.1	PCA	
JL4	J2	24.3	99.6	150/49	11/11	40.7	3.2	36.1	4.5	227.0	3.0	79.4	2.7	36.0	3.7	329.3	2.5	4.6	18.1	GC+PCA	
JL5	J2	24.3	99.6	158/45	14/14	37.5	1.8	41.1	2.2	599.3	1.6	84.7	2.3	47.3	2.4	401.1	2.0	4.2	15.6	GC+PCA	
JL6	J2	24.3	99.6	160/51	11/12	42.2	3.6	40.2	4.5	191.4	3.3	92.4	3.8	42.9	4.5	172.9	3.5	4.6	18.1	PCA	
JL7*	J2	24.2	99.7	271/46	9/9	337.7	11.1	44.8	12.5	27.8	9.9	313.9	8.7	16.7	16.1	37.2	8.6	5.0	20.5	GC+PCA	
JL8*	J2	24.2	99.7	280/37	9/9	358.7	6.6	55.2	5.3	323.8	5.3	323.8	4.9	36.1	6.8	125.4	4.6	5.0	20.5	PCA	
JL9*	J2	24.2	99.7	280/37	8/9	1.9	7.8	58.5	4.2	58.5	5.4	322.1	4.2	39.5	5.4	202.6	3.9	5.2	22.1	PCA	
JL10*	J2	24.2	99.7	266/32	9/9	338.3	3.9	57.7	2.8	283.5	3.1	306.9	2.3	39.1	3.0	599.2	2.1	5.0	20.6	PCA	
Mean JL1-6 (site averages)					6/6	38.8	4.5	40.5	5.7	258.5	4.2	80.3	7.2	40.0	9.2	102.1	6.7	2.2	5.6		
Mean JL1-6 (directions)					71/72	38.9	1.6	40.6	2.0	158.8	1.5	79.5	2.2	39.3	2.0	66.9	2.1	2.2	5.6		
Mean JL7-10 (site averages)*					4/4	348.4	17.0	54.6	13.9	45.1	13.8	317.6	10.1	32.2	15.1	92.7	9.6	2.9	8.7		
Mean JL7-10 (directions)*					35/36	348.1	5.2	54.5	4.3	33.6	4.2	316.5	3.7	33.0	5.5	47.7	5.5	2.9	8.7		
Paleocene Muguahue Formation																					
MG1	E1	24.2	99.3	76/41	12/12	229.0	10.8	-43.6	12.5	21.0	9.7	236.7	6.8	-5.6	13.5	41.6	6.8	4.4	17.1	GC+PCA	
MG2	E1	24.2	99.3	75/34	13/13	250.9	6.8	-31.3	13.5	20.5	9.4	251.5	8.0	2.6	15.9	28.0	8.0	4.3	16.3	GC+PCA	
MG3	E1	24.2	99.3	92/24	11/11	255.9	6.6	-30.6	10.3	52.4	6.4	258.1	5.7	-7.4	11.2	65.9	5.7	4.6	18.1	GC+PCA	
MG4	E1	24.2	99.3	103/44	13/13	288.7	5.5	-36.7	7.5	66.9	5.1	287.6	4.3	7.1	8.5	94.2	4.3	4.3	16.3	GC+PCA	
MG5	E1	24.2	99.3	89/47	12/12	223.1	9.3	-45.3	10.3	28.1	8.3	238.4	7.2	-7.3	14.2	37.3	7.2	4.4	17.1	GC+PCA	
MG6	E1	24.3	99.3	90/49	10/10	303.9	5.2	-8.5	10.3	86.6	5.2	310.3	4.4	31.5	6.7	132.7	4.2	4.8	19.2	GC	
MG7	E1	24.2	99.3	83/77	12/12	313.7	15.2	69.6	6.1	24.2	9.0	65.7	5.7	25.2	9.5	62.8	5.5	4.4	17.1	GC+PCA	
MG8	E1	24.2	99.3	80/66	9/12	281.6	14.6	-21.6	25.7	11.1	14.3	278.5	14.2	35.9	19.8	15.8	13.4	5.0	20.5	GC+PCA	
MG9	E1	24.2	99.3	62/61	10/13	348.2	9.0	82.6	9.1	8.8	17.3	54.0	8.5	26.7	14.0	35.1	8.3	4.8	19.2	GC+PCA	
MG10	E1	24.2	99.3	74/42	10/11	44.7	19.8	45.0	22.0	8.5	17.6	53.6	12.5	6.4	24.8	15.9	12.5	4.8	19.2	GC+PCA	
Tilt-Corrected																					
In Situ																					
Site	Age	Lat (°N)	Long (°E)	Bedding Dip/Dip(°)	n/n ₀	D _g (°)	ΔD _x (°)	I _g (°)	ΔI _x (°)	K	A ₉₅	D _s (°)	ΔD _x (°)	I _s (°)	ΔI _x (°)	K	A ₉₅	A _{95min}	A _{95max}	Method	
Paleocene Muguahue Formation (Tong et al., 2016)																					
YP2#	E2	24.2	99.3	106/27	8/12	251.1	10.8	-33.6	12.5	21.0	9.7	236.7	6.8	-5.6	13.5	41.6	6.8	4.4	17.1	GC+PCA	
YP4#	E3	24.2	99.3	271/37	9/13	262.7	19.6	19.6	19.6	19.6	19.6	262.9	19.6	-17.1	17.1	20.2	14.3	2.2	5.6	GC+PCA	
YP10#	E4	24.2	99.3	76/46	10/15	236.6	-54.1	-54.1	-54.1	-54.1	-54.1	244.6	-54.1	-9.5	9.5	13.9	15.4	1.9	4.6	GC+PCA	
YP11#	E5	24.2	99.3	74/59	9/11	151.4	81.5	81.5	81.5	81.5	81.5	83.5	81.5	28.8	28.8	37.2	12.1	2.2	5.6	GC+PCA	
YP12#	E6	24.2	99.3	89/61	7/12	29.0	29.0	29.0	29.0	29.0	29.0	77.3	29.0	22.3	22.3	69.4	10.2	2.2	5.6	GC+PCA	
Mean MG1-10 (site averages)					7/10	72.2	21.7	41.0	26.8	10.3	19.8	70.9	14.1	5.2	28.0	14.3	14.1	2.2	5.6		
Mean MG1-10 (directions)					9/10	73.1	5.6	40.8	7.0	11.8	5.2	70.6	4.1	6.8	8.2	13.2	4.1	1.9	4.6		
Mean with Tong et al. (2016; site averages)					96/119	72.2	16.2	36.2	2.4	11.1	15.1	73.1	9.1	9.9	17.7	20.2	9.1	1.9	4.6		
Mean with Tong et al. (2016; site averages)					14/15																
Mean with Tong et al. (2016; Directions)					96/162	70.9	5.2	41.2	6.5	10.0	4.8	72.5	3.3	10.0	6.5	14.0	3.3	1.7	3.7		
Mean with Tong et al. (2016; directions)					139/162																

Note. Lat/Long: site latitude/longitude; n/n₀: specimens used for statistical/demagnetized; D_g(D_s)/I_g(I_s): declination/inclination in *in situ* and tilt-corrected coordinates; ΔD_x: error on declination; ΔI_x: error on inclination. Statistical parameters are given by a confidence cone using Fisher (1953) statistics on virtual geomagnetic poles (A₉₅, K). A_{95min} and A_{95max} correspond to the confidence envelope of Deenen et al. (2011). GC: great circle; PCA: principle component analysis. * and # denote sites of Group B from Jurassic and sites from Tong et al. (2016), respectively.

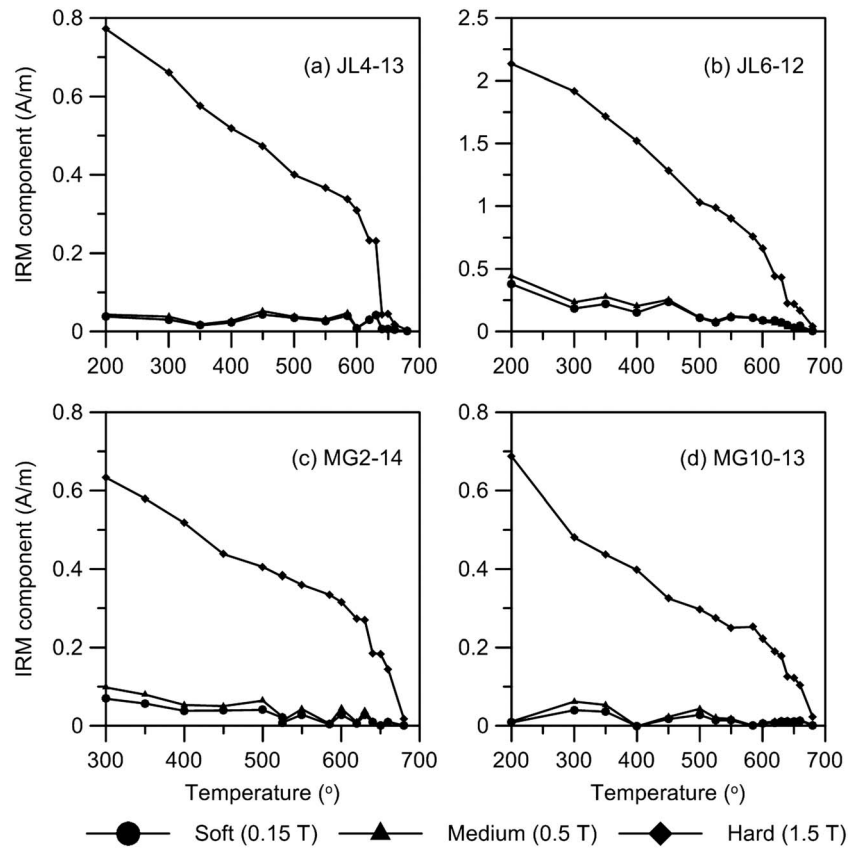


Figure 3. Thermal demagnetization of the composite isothermal remanent magnetization (IRM; imparted with direct current fields of 1.5 T, 0.5 T, and 0.15 T along three perpendicular axes) from (a, b) the Jurassic and (c, d) the Paleocene sediments.

(Figures 5d and 5e), which is similar from what we observed from the early Cenozoic red beds in the Jinggu Basin (Li, Yang, et al., 2017), suggesting a secondary origin.

4.3. Demagnetization Results

4.3.1. Paleomagnetic Results for the Jurassic Luzijing Formation

The natural remanent magnetization (NRM) intensities of Luzijing Formation rocks are between 1.52×10^{-3} and 2.24×10^{-4} A/m. The demagnetization behavior of specimens from the Luzijing Formation is divided into two types. For the first type, demagnetization diagrams (78 specimens, 75%) show a linear decay of NRM intensity toward the origin with increasing temperature steps (Figures 6b–6e). In this case, the high-temperature component (HTC), interpreted as the characteristic remanent magnetization (ChRM), was isolated between temperatures of 610°C and 680°C. The second type of demagnetization behavior displays well-defined great circle paths below temperatures of 650°C as shown on stereographic plots (Figures 6a and 6f). In this situation, a great circle approach was used to calculate the site mean direction based on the method of McFadden and McElhinny (1988). Where great circles were used on sites or localities with nonhomogenous bedding, great circle analysis was performed in geographic and tectonic coordinates separately, as the optimal direction chosen on a great circle is different in both coordinates (standard procedure on Paleomagnetism.org; Koymans et al., 2016). A low-temperature component (LTC) was isolated in most specimens mostly at temperature intervals of 25°C to 250°C.

The site mean directions for the Luzijing Formation are clearly plotted into two groups in both the LTC and the ChRM (Figure 7). One group (A) includes sites JL1–6 sampled in the north and gives in geographic coordinates a mean direction of $Dec \pm \Delta D_x = 38.9 \pm 1.6^\circ$, $Inc \pm \Delta I_x = 40.6 \pm 2.0^\circ$, and in tectonic coordinates a mean direction of $Dec \pm \Delta D_x = 79.5 \pm 2.2^\circ$, $Inc \pm \Delta I_x = 39.3 \pm 2.0^\circ$ ($n = 71$, $K = 66.9$, $A_{95} = 2.1^\circ$,

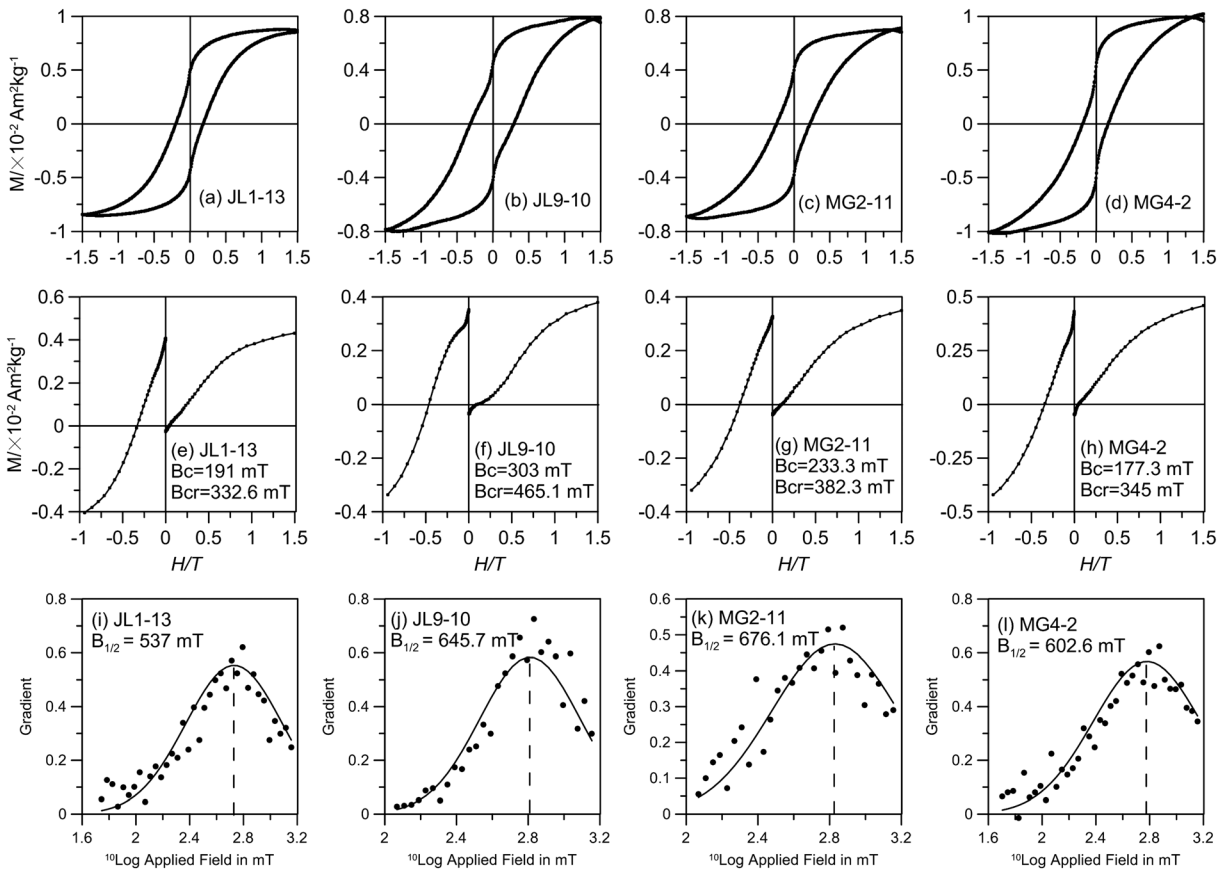


Figure 4. Hysteresis loops (a–d), isothermal remanent magnetization (IRM) acquisition, back-field demagnetization curves (e–h), and IRM component analysis (i–l) (Kruiver et al., 2001) of representative samples from the Jurassic and Paleocene sediments.

$A_{95min,max} = [2.2, 5.6]$). Group (B) includes sites JL7–10 sampled ~15 km to the south (Figure 2) and gives in geographic coordinates a mean direction of $Dec \pm \Delta D_x = 348.1 \pm 5.2^\circ$, $Inc \pm \Delta I_x = 54.5 \pm 4.3^\circ$, and in tectonic coordinates a mean direction of $Dec \pm \Delta D_x = 316.5 \pm 3.7^\circ$, $Inc \pm \Delta I_x = 33.0 \pm 5.5^\circ$ ($n = 35$, $K = 47.7$, $A_{95} = 5.5^\circ$, $A_{95min,max} = [2.2, 5.6]$). The detailed mean directions of Group A and Group B are presented in Table 1 and Figure 7.

4.3.2. Paleomagnetic Results for the Paleocene Muguah Formation

The specimens of the Muguah Formation have NRM intensities from 5.31×10^{-4} to 5.88×10^{-3} A/m. A few (38) specimens show linear character in the high temperature (e.g., Figure 6i), and the ChRMs were isolated by least-squares fits. Most specimens, however, exhibit well-defined great circle paths at temperatures lower than 650–670°C as shown on the stereographic plot (Figures 6j–6k). Each site mean direction is calculated according to the method of McFadden and McElhinny (1988). A LTC is generally isolated below the temperatures of 300°C and shows near-random directions interpreted as a viscous overprint (Figure 8a). The site mean directions for the Muguah Formation are of dual polarity (Figure 8b); after inverting the reversed polarity directions, they have in geographic coordinates a mean direction of $Dec \pm \Delta D_x = 73.1 \pm 5.6^\circ$, $Inc \pm \Delta I_x = 40.8 \pm 7.0^\circ$ ($n = 71$, $K = 11.8$, $A_{95} = 5.2^\circ$, $A_{95min,max} = [2.2, 5.6]$) and in tectonic coordinates a mean direction of $Dec \pm \Delta D_x = 70.6 \pm 4.1^\circ$, $Inc \pm \Delta I_x = 6.8 \pm 8.2^\circ$ ($n = 96$, $K = 13.2$, $A_{95} = 4.1^\circ$, $A_{95min,max} = [1.9, 4.6]$; Figure 8). Tong et al. (2016) reported data from five sites from the Muguah Formation exposed a few kilometers north from our sampling area and combining our data with parametrically sampled data from the site averages reported by Tong et al. (2016) yield a mean direction of the Paleocene Muguah Formation in geographic coordinates of $Dec \pm \Delta D_x = 70.9 \pm 5.2^\circ$, $Inc \pm \Delta I_x = 41.2 \pm 6.5^\circ$ ($n = 96$, $K = 10$, $A_{95} = 4.8^\circ$, $A_{95min,max} = [1.9, 4.8]$) and in tectonic coordinates a mean direction of $Dec \pm \Delta D_x = 72.5 \pm 3.3^\circ$, $Inc \pm \Delta I_x = 10.0 \pm 6.5^\circ$ ($n = 139$, $K = 14$, $A_{95} = 3.3^\circ$, $A_{95min,max} = [1.7, 3.7]$).

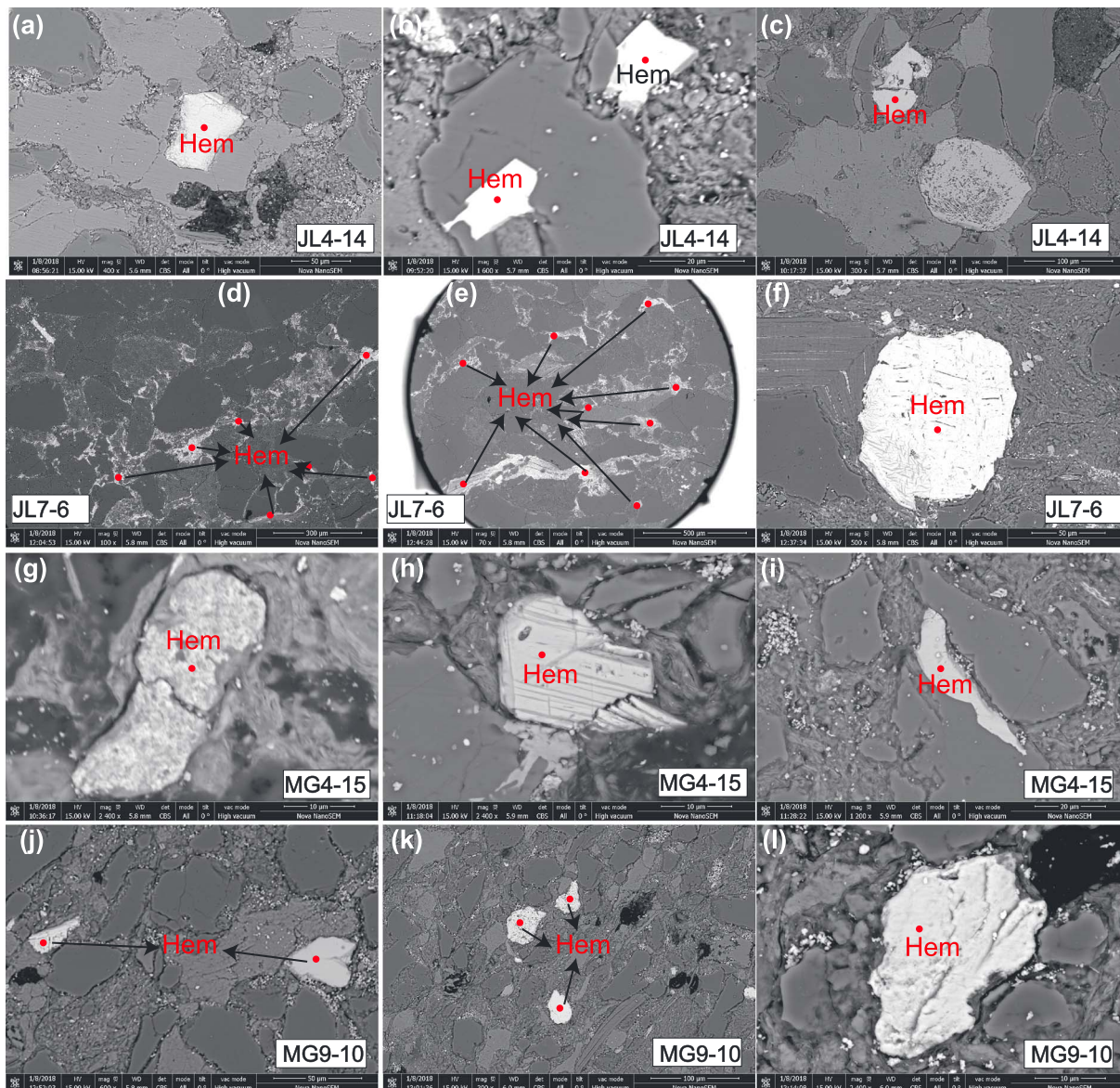


Figure 5. SEM backscattered electron images for selected specimens of the Jurassic Luzijing (JL4-14 (a–c) and JL7-6 (d–f)) and Paleocene Muguahé (MG4-15 (g–i) and MG9-10 (j–l)) Formations. Hem: hematite.

5. Discussions

5.1. Reliability of the Paleomagnetic Directions

The classical fold tests (Tauxe & Watson, 1994) and reversals test (McFadden & McElhinny, 1990) were employed to assess the primary nature of the paleomagnetic directions we isolated. For the Jurassic Luzijing Formation, the directions of Group A and Group B are clearly significantly different before and after tilt correction and yield a negative fold test. However, close inspection of the demagnetization diagrams of the Group B sites shows that these samples have a very large LTC that is unblocking up to temperatures of 550°C (Figure 6f), but in some cases, a higher temperature component shows that another component is present, although it cannot be resolved in detail. The ChRM directions of Group B are close to the present dipole field direction before tilt adjustment (Figure 7), and the SEM results suggest a secondary origin of the hematite in this group (Figures 5d and 5e). We, therefore, interpret that the directions derived from Group B are a recent remagnetization.

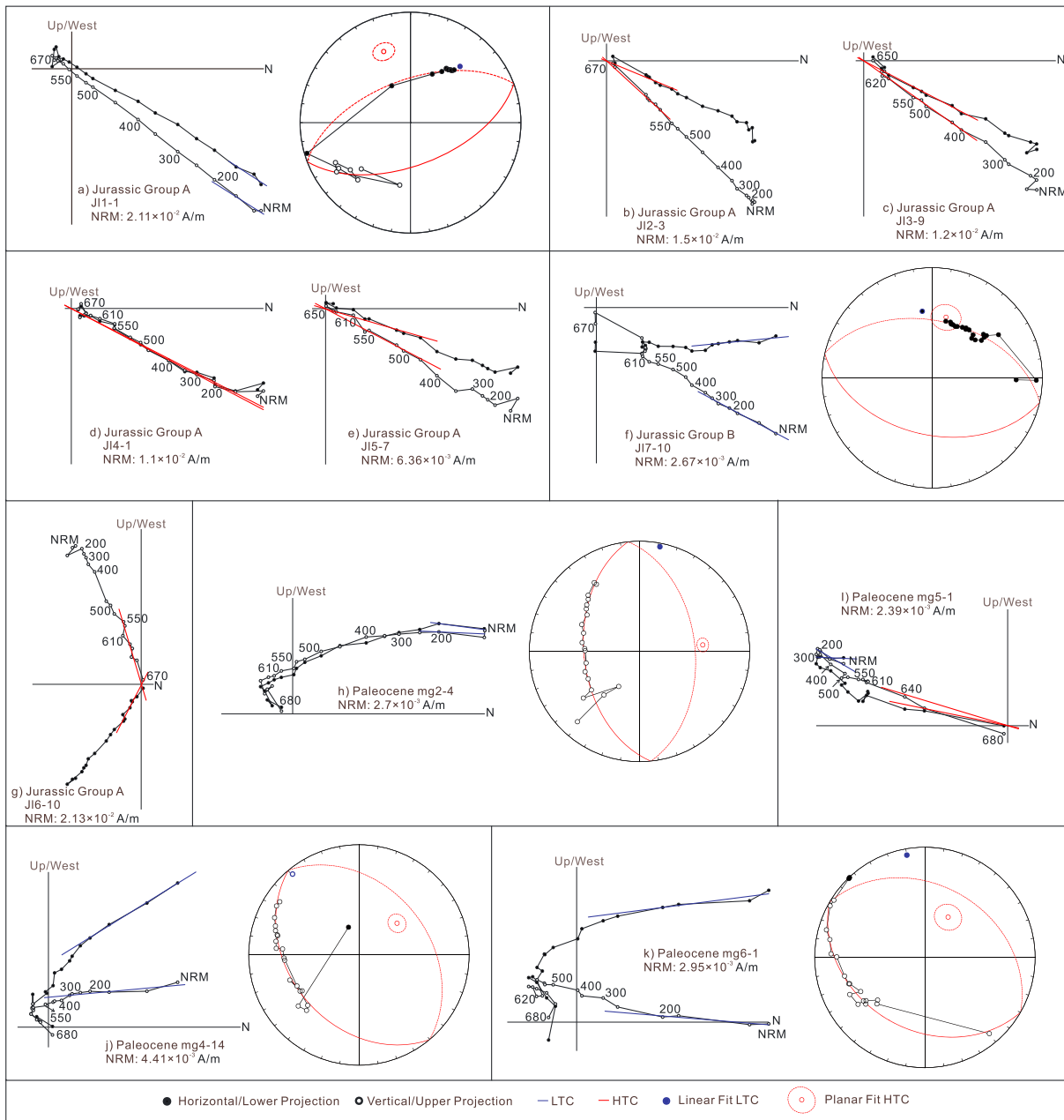


Figure 6. Orthogonal vector projections of demagnetization for (a–g) Jurassic and (h–k) Paleocene specimens in geographical coordinates. Solid and open symbols refer to vector projected onto the horizontal and vertical planes, respectively. NRM: natural remanent magnetization.

The ChRM of Group A is based on six sites from a monoclinical section and records five normal polarity and one reversed polarity mean directions (Figure 7b). Although the fold test on the six sites of Group A is inconclusive when performed on site averages and negative when performed on directions (Figure 9a), we suggest a primary origin of the ChRM of Group A based on the following evidences. First, the directions of ChRM deviate strongly from the recent field in both *in situ* and *tilt-corrected* coordinates, and a recent overprint is thus excluded. Second, the normal and reversed polarity directions pass the reversals test with a C classification (McFadden & McElhinny, 1990). Third, the inclinations of Group A before and after tilt correction coincide with the expected inclination for the Qiangtang terrane after collision with Eurasia (Torsvik et al., 2012) and thus form no basis to identify a remagnetization. Fourth, the SEM results indicate a detrital origin of hematite in Group A (Figures 5a–5c). Finally, Huang and Opdyke (1993) reported results from Middle Jurassic rocks near Luxi, ~100 km to the west of the present study area (Figure 1). The bedding attitudes at these two localities

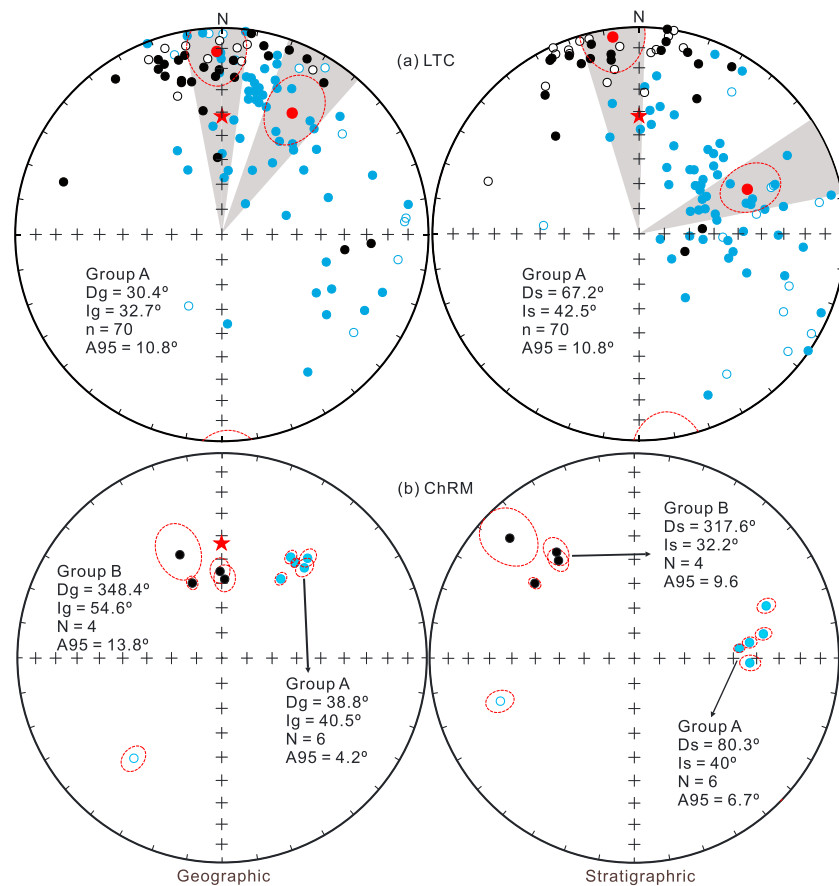


Figure 7. Equal-area projections of the site mean directions of the (a) low-temperature component (LTC) and (b) characteristic remanent magnetization (ChRM) for the Jurassic Luzijing Formation in *in situ* (left) and *tilt-corrected* (right) coordinates. Solid (open) symbols refer to positive, downward (negative, upward) inclinations; red dot indicates overall mean direction with 95% confidence limits; and red star denotes the geocentric axial dipole field direction at the sampling site. The blue and black colors represent the Group A and Group B directions, respectively.

are distinctly different, which permit a regional fold test. As shown in Figure 9c, the regional fold test combining our data with those of Huang and Opdyke (1993) is positive. Therefore, we interpret that the magnetization from the six sites of Group A is primary, and there has been an $\sim 80^\circ$ clockwise rotation since the Middle Jurassic.

The Paleocene Mugahe Formation yielded an inconclusive fold test (Tauxe & Watson, 1994) suggesting optimal clustering at $>150\%$ unfolding (Figure 9b). The normal and reversed polarity directions do pass the reversals test with a C classification (McFadden & McElhinny, 1990). Also combining our data with those of Tong et al. (2016) yields a positive fold test, with optimal clustering between 77% and 119% unfolding (Figure 9d). The SEM results indicate that the hematite in the Mugahe Formation is a detrital origin (Figures 5g–5l). These lines of evidences indicate that the magnetization isolated from the Paleocene Mugahe Formation is most likely primary. The declination derived from the Paleocene rocks is almost equal before and after tilt correction, 73.1 ± 5.6 versus 70.6 ± 4.1 , showing that the region has undergone a major post-Paleocene vertical axis rotation. The inclination in geographic and tectonic coordinates, however, is very different. In geographic coordinates, the inclination is $\sim 35\text{--}40^\circ$, suggesting a paleolatitude of $\sim 20^\circ$, which is consistent with the predicted paleolatitude from Paleocene to today by reconstructions in a paleomagnetic reference frame (Torsvik et al., 2012). In tectonic coordinates, however, the inclination is $7\text{--}10^\circ$, depending on whether sites or samples are averages and whether paleomagnetic data of Tong et al. (2016) are included or not. This suggests a latitude close to the equator, whereas the study area has quite certainly never been at such low latitudes since the Paleocene. The anomalous low inclination than expected might be attributed to a combined effect of inclination shallowing of red beds, which is a very common feature of sediments (e.g., Li et al., 2013),

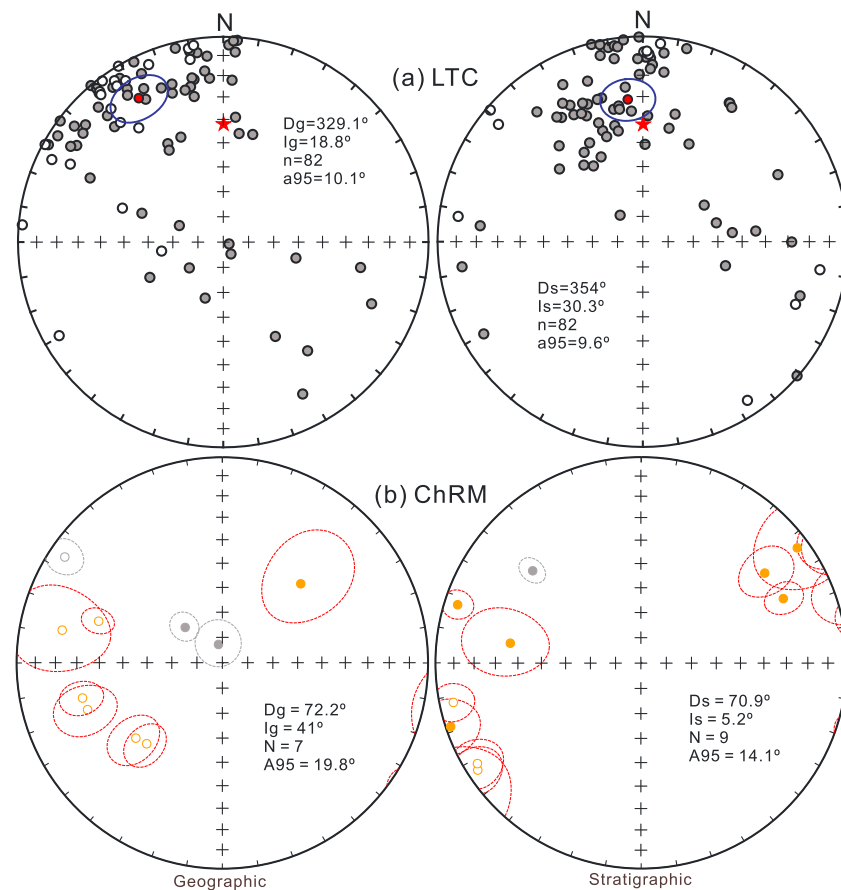


Figure 8. Equal-area projections of the site mean directions of the (a) low-temperature component (LTC) and (b) characteristic remanent magnetization (ChRM) for the Paleocene Muguahé Formation in *in situ* (left) and *tilt-corrected* (right) coordinates. The gray dots in Figure 8b represent the sites that were excluded from calculating the mean direction. The other symbols are the same as in Figure 7.

the folding of Muguahé Formation between early Miocene and Oligocene, and deformations of left-lateral strike slip faults around late Miocene.

5.2. Rotation Pattern of Northern Sibumasu as Indicated by Paleomagnetism

Huang and Opdyke (1993) obtained a HTC and ITC (intermediate temperature component) from the Middle Jurassic Mengga Formation in Luxi. However, neither fold nor reversal tests were applied for these paleomagnetic data, which makes it hard to recognize whether these paleomagnetic results are reliable or not. Tong et al. (2016) suggested that both their HTC and ITC are remagnetized components from the Miocene and after Miocene, respectively. However, the positive regional fold test of paleomagnetic results from the Middle Jurassic Mengga and Luzijing Formation suggest that the HTC from both the Mengga and Luzijing Formation are representative for the Middle Jurassic characteristic paleomagnetic directions from the northern Sibumasu area. Huang and Opdyke (1993) speculated that the ITC of the Middle Jurassic Mengga Formation was a mid-Cretaceous overprint, because the paleopoles determined from the ITC overlap with the poles from the middle Cretaceous Manggang Formation in the Simao Basin to the east. However, as noted by Tong et al. (2016) and Li, Advokaat, et al. (2017), the paleomagnetic directions in the Simao Basin are highly variable, and it is far from robust to confirm that the ITC of Middle Jurassic Mengga Formation is a Middle Cretaceous overprint based solely on the similarity of paleopoles. Interestingly, the ITC of the Mengga Formation ($D_s = 60.9^\circ$, $I_s = 32.0^\circ$) is roughly similar with the LTC of the Luzijing Formation ($D_s = 67.2^\circ$, $I_s = 42.5^\circ$), suggesting that both of them represent a later remagnetization, but the remagnetization time is uncertain. Tong et al. (2016) also found a remagnetization from Oligocene sediments in Changning. Recently, we found a prefolding remagnetization from Paleocene-Oligocene sediments in the

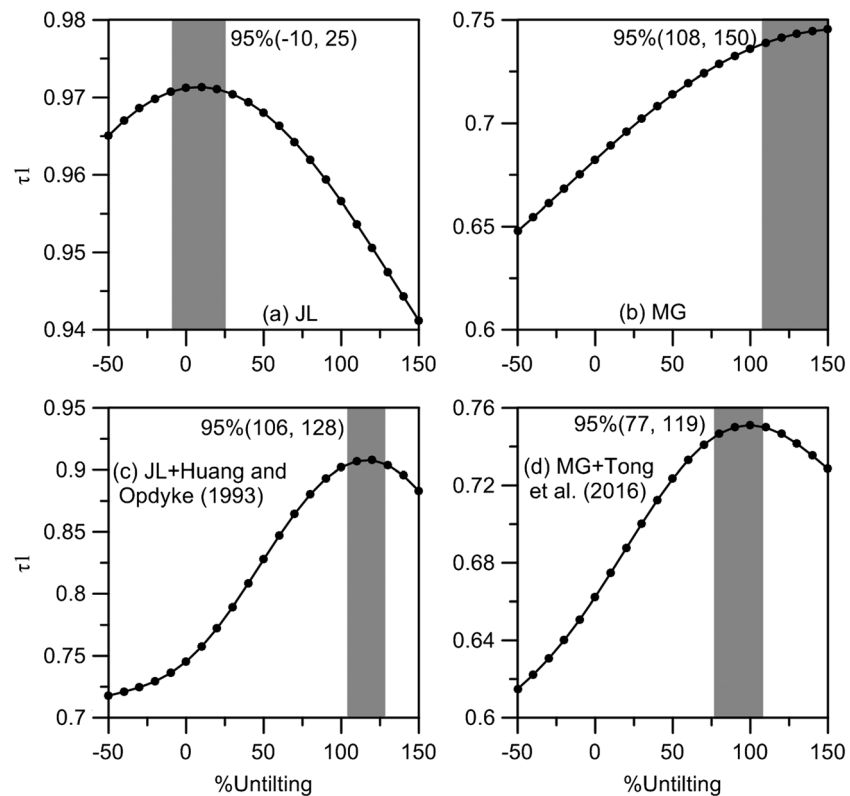


Figure 9. Nonparametric fold tests (Tauxe & Watson, 1994) of paleomagnetic results on directions of (a) Middle Jurassic Luzijing Formation, (b) Paleocene Mugahe Formation, (c) Middle Jurassic Luzijing Formation of this study and Mengga Formation in Luxi (Huang & Opdyke, 1993), and (d) Paleocene Mugahe Formation of this study and Tong, et al. (2016). Results of the fold test come with bootstrapped statistics on the first eigenvalues (τ_1) upon progressive untilting. The 95% bootstrap error interval is indicated above each panel.

Jinggu Basin, located in the middle part of the Indochina Block (Li, Yang, et al., 2017). The folding time of these sediments is in the late Oligocene, which precisely constrained the remagnetization in Oligocene. The Oligocene remagnetization is in time consistent with Oligocene surface uplift, widespread hydrothermal mineralizations, which may in turn be linked to processes driving extrusion of the whole of the Indochina Block. Kornfeld, Eckert, Appel, Ratschbacher, Pfandere, et al. (2014) reported a remagnetization from the Permian mata-basalt in Liuku, which was heated and cooled around ~ 30 Ma as suggested by $^{40}\text{Ar}/^{39}\text{Ar}$, suggesting that the remagnetization occurred at this time. We therefore suspect that all of these remagnetization events may have occurred in Oligocene.

Kornfeld, Eckert, Appel, Ratschbacher, Sonntag, et al. (2014) identified two groups of paleomagnetic directions from ~ 50 – 35 Ma mafic dykes in Pianma. They suggested that Group 1 carried by Ti-rich titanomagnetite with large declination ($D/I = 89.8^\circ/35.1^\circ$) is primary and Group 2 carried by magnetite with moderate declination ($D/I = 33.3^\circ/41.4^\circ$) is secondary. However, as noted by the authors, samples from Group 1 probably do not sufficiently sample PSV and may represent a spot reading of the geomagnetic field. They found no indication for remagnetization of their Group 2. Considering that the paleomagnetic direction of Group 2 is consistent with that from Liuku ($D/I = 42.2^\circ/47^\circ$; Kornfeld, Eckert, Appel, Ratschbacher, Pfandere, et al., 2014), which is only a few kilometers southeast of Pianma, we thus considered Group 2 as the primary direction from the Pianma mafic dykes. Other reliable paleomagnetic data from northern Sibumasu include the Paleocene Mugahe Formation (Tong et al., 2016) and Lower Pliocene to Holocene volcanics in Mangbang (Kornfeld, Sonntag, et al., 2014). However, the paleomagnetic directions from the Lower Pliocene to Holocene volcanic were suggested to reflect the activity of local normal fault (Kornfeld, Sonntag, et al., 2014) and therefore cannot be used to determine the regional rotation of Sibumasu. Paleomagnetic data from the other areas are compiled in Li, Advokaat, et al. (2017).

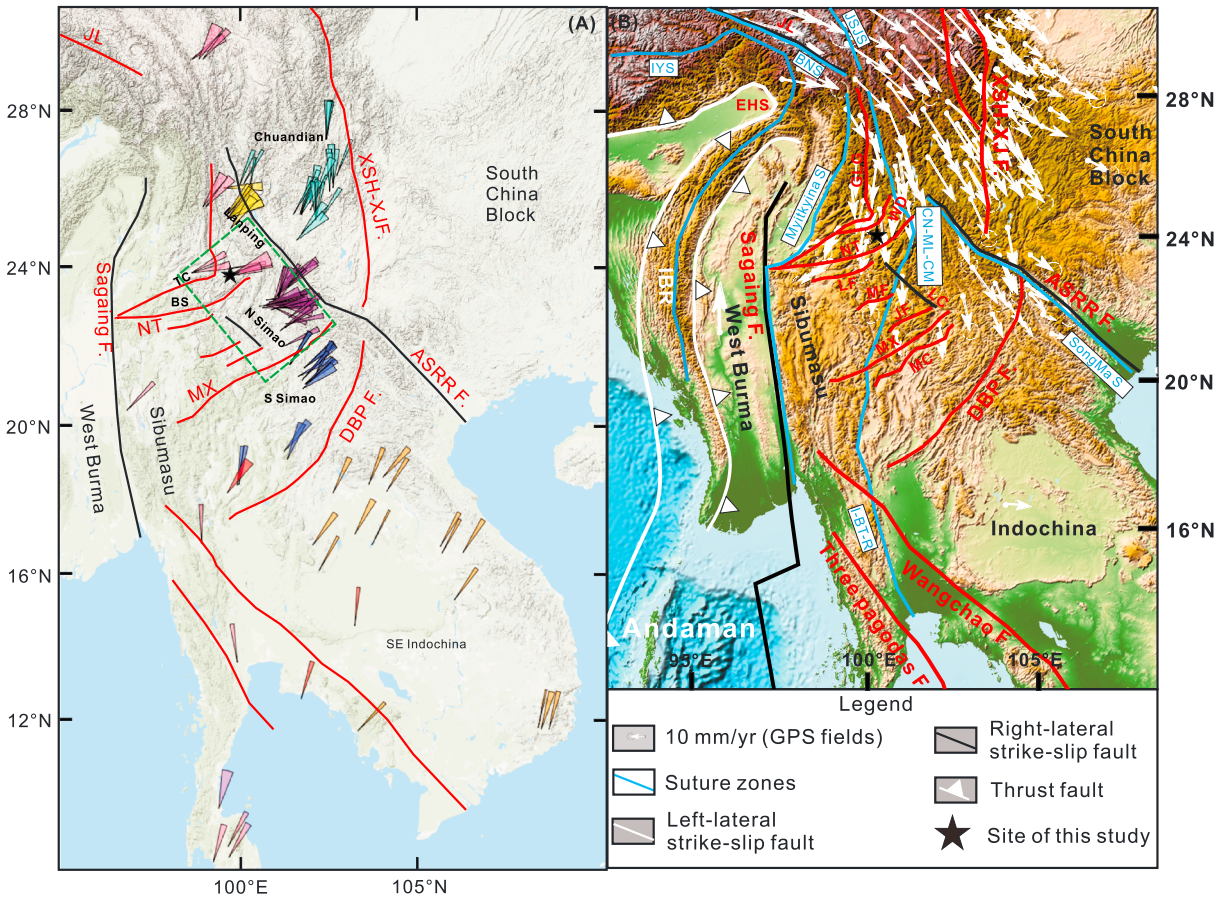


Figure 10. (a) Map with locations and declinations of the paleomagnetic sites marked with different colors showing the rotation pattern of southeast margin of the Tibetan Plateau (data files are provided in the supporting information compatible with Paleomagnetism.org). (b) The GPS velocity field around the southeast margin of the Tibetan Plateau. The cyan represents the Chuandian terrane. The orange, blue, purple, and yellow represent the four subterrane of Southeast (SE) Indochina, Southern (S) Simao, Northern (N) Simao, and Lanping, respectively. The pink represents data from the Sibumasu Block (see Li, Advokaat, et al., 2017, for detailed information). The red represents paleomagnetic data from rare volcanic or plutonic sites. The black star represents the site of this study. The red and black lines represent the main left-lateral and right-lateral faults, respectively. The blue lines represent the main sutures in the southeast margin of the Tibetan Plateau. The green square represents the area that underwent a large clockwise rotation as indicated by paleomagnetic directions. The abbreviations are the same as in Figure 1.

The inferred rotations of northern Sibumasu are shown in Figure 10a. Paleomagnetic results suggest a ~40° clockwise rotation in the Three Rivers region, where the faults trend N-S, and a ~60–80° clockwise rotation of Tengchong and Baoshan, where the faults trend NE–SW.

5.3. Tectonic Implications of the Tibetan Plateau Evolution

Although present GPS data suggest that the crustal material in southeastern Tibet moves southwestward beyond the southern limit of the Xianshuihe-Xiaojiang fault with a clockwise rotation (Figure 10b), it remains unclear where the transfer of crust from Tibet is accommodated to the south of the Ailao Shan-Red River fault. Our paleomagnetic results together with geologic evidences may allow a first-order test on whether this motion may have been accommodated south of the Ailao Shan-Red River fault.

Paleomagnetic data from the Baoshan area along with previously published data in northern Sibumasu reveal a significantly large (~70–80°) clockwise rotation of northern Sibumasu with respect to Eurasia (Figure 10a). Our recent review on paleomagnetic data from Indochina Block showed that the northern Simao also experienced a ~60–80° clockwise rotation (Li, Advokaat, et al., 2017; Figure 10a). This suggests that the area lying southwest of the Ailao Shan-Red River fault and sandwiched between Mengxing and Gaoligong faults (green square in Figure 10a) experienced a significant large clockwise rotation. Interestingly, this area is also the place where the curved left-lateral strike-slip faults are developed. These NE-striking strike-slip faults initiated at late Miocene and have accumulated displacements of ~90 km

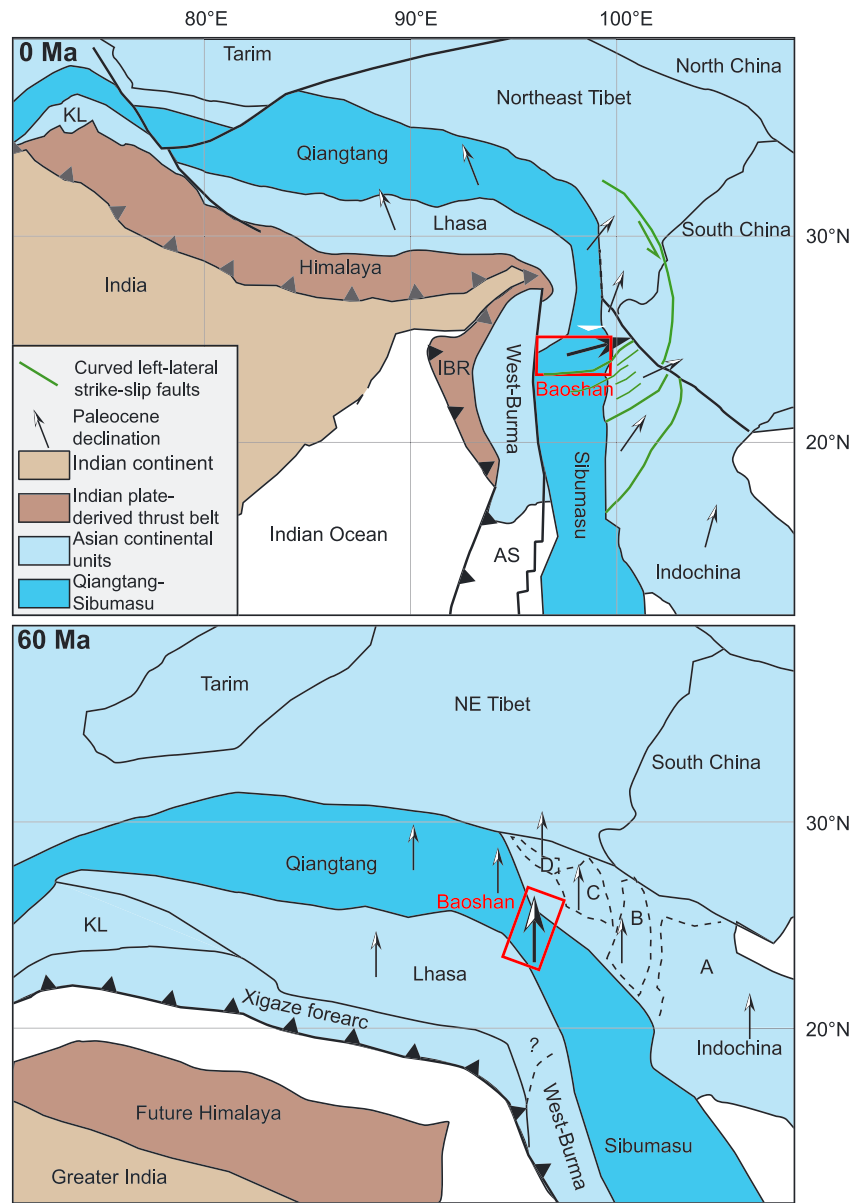


Figure 11. Restored position of the strongly rotated Baoshan region analyzed in this paper in context of the regional kinematic evolution of Tibet and Southeast Asia. Reconstruction at 60 Ma placed in a paleomagnetic reference frame based on the GAPWaP of Torsvik et al. (2012). AS = Andaman Sea, IBR = Indo-Burman ranges, KL = Kohistan-Ladakh arc. Arrows indicate paleomagnetic declinations (see paleomagnetic data compilations in Li, Advokaat, et al., 2017). Green lines represent the curved left-lateral strike-slip faults. A, B, C, and D represent the four subterraces defined in Li, Advokaat, et al. (2017): Southeast Indochina, Southern Simao, Northern Simao, and Lanping.

(Wang et al., 2014), which is almost equal to the displacement (80–100 km) along the Xianshuihe-Xiaojiang fault. Given the similar age, displacements, and strike between the Xianshuihe-Xiaojiang fault and these NE–SW strike-slip faults, and present GPS velocity field (Zhang et al., 2004), these data suggest that the shear accommodated along the Xianshuihe-Xiaojiang fault is in the southwest transmitted toward Myanmar (Burchfiel et al., 2007).

This hypothesis is also supported by the paleomagnetic data. Our previous reconstruction suggested that the northern Simao experienced a ~65° clockwise rotation in the Eocene-middle Miocene time associated with extrusion (Li, Advokaat, et al., 2017). The Baoshan region, west of the curved fault systems, may have accommodated up to a 80° clockwise rotation. This indicates an up to 15° additional rotation after the

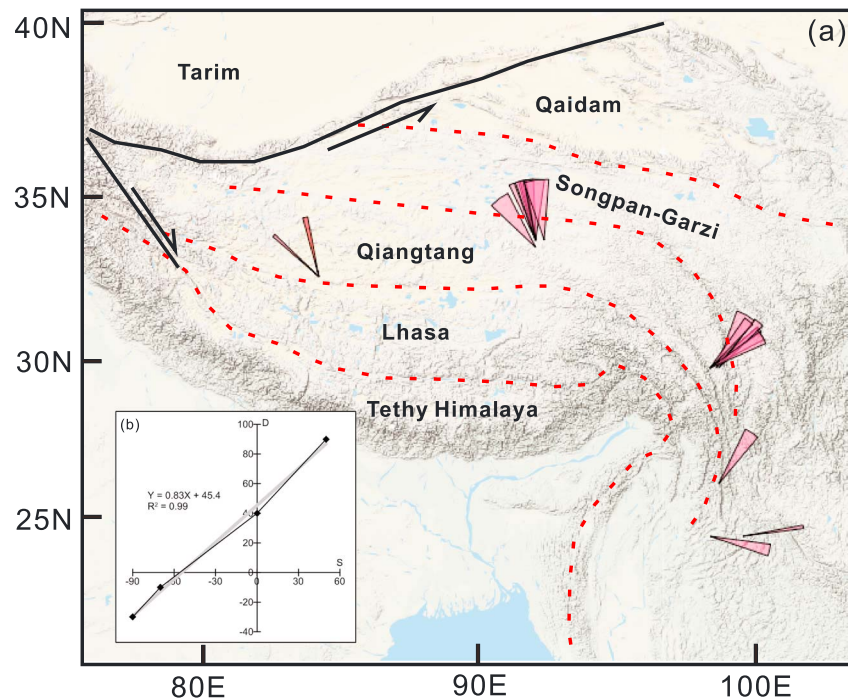


Figure 12. Compiled paleomagnetic declination (D) from Qiangtang/northern Sibumasu showing variable rotation (a) and can be well correlated with the strike (S) of Qiangtang/northern Sibumasu (b). The expected strike of Qiangtang/northern Sibumasu before rotation is N60°W.

middle Miocene, which is almost equal to the paleomagnetically determined rotation degree from the middle Miocene strata of the Simao basin (Gao et al., 2015; Li, Yang, et al., 2017) and Neogene sediments from the Chuandian terrane (Gao et al., 2017; Li et al., 2013; Zhu et al., 2008). These would suggest a clockwise rotation rate of $\sim 1^\circ/\text{Myr}$ of the west of the curved fault area since middle Miocene, which is also consistent with GPS result (Zhang et al., 2004). Therefore, we tentatively suggest that the northern Sibumasu and northern Simao first experienced a $\sim 65^\circ$ clockwise rotation during the early Cenozoic of Indochina extrusion and may have undergone a further $\sim 10\text{--}15^\circ$ clockwise rotation after the late Miocene during the eastward motion of Tibet crust, which was accommodated by Longmen Shan thrusting in eastern Tibet, and by rotational outflow in southeastern Tibet toward Myanmar (Figure 11).

5.4. Paleogeography of Qiangtang Block in Jurassic

The Sibumasu Block represents an eastern extension of Qiangtang Block. Our Jurassic paleomagnetic data from the Baoshan area of northern Sibumasu therefore provide an opportunity to reconstruct the paleogeography of the eastern Qiangtang Block prior to the India-Asia collision. Recently, we updated the previous kinematic restoration of Tibet of van Hinsbergen et al. (2011) by including the paleomagnetism-based restoration of Indochina extrusion of Li, Advokaat, et al. (2017), which required a considerably larger amount of Indochina extrusion along the eastern Jinshajiang suture. This larger extrusion predicted that the eastern Lhasa and Qiangtang terranes underwent a $\sim 20^\circ$ counterclockwise rotation since the Paleocene (Figure 11), which is supported by the compiled paleomagnetic data from Lhasa and Qiangtang (Chen et al., 2017; Yan et al., 2016, Figure 12). We compiled paleomagnetic data from the Jurassic and Cretaceous of northern Sibumasu (e.g., Huang et al., 1992; Otofujii et al., 1990; Tong et al., 2015; supporting information Table S1), showing a $\sim 40^\circ$ clockwise rotation around the eastern Himalaya syntaxis and as much as $\sim 90^\circ$ clockwise rotation in northern Sibumasu (Figure 10a), which is supported by our data. After rotating these areas back according to their paleomagnetic declinations, the strike of the Qiangtang terrane and bounding Bangong-Nujiang suture would be restored to a NW-SE direction, suggesting that the southern margin of Qiangtang Block was a straight or slightly bent structure prior to the construction of the Tibetan Plateau, with an orientation of $\sim \text{N}60^\circ\text{W}$ (Figure 11). Fujiwara et al. (2014) found that the southern Sibumasu was also originally a straight structure with a general trend of $\text{N}10^\circ\text{W}$ based on the paleomagnetic data from southern

Sibumasu, which would suggest that there is a 50° turn between the Qiangtang/northern Sibumasu and southern Sibumasu (Figure 11). Such a ~50° bend is also consistent with the strike of the main Neotethys slab in the lower mantle (Replumaz et al., 2004, 2010).

The reconstructed paleogeography of Qiangtang Block is also supported by the paleolatitude data, although with some uncertainties of inclination shallowing of sediments. The paleolatitude of the westernmost Qiangtang Block in Gaize area, derived from volcanic rocks and inclination-corrected red beds, is ~30°N (Chen et al., 2017). The paleolatitude of the central Qiangtang Block from the Yanshiping area, derived from limestones and sandstones, is ~16–22°N (without inclination-shallowing correction; Yan et al., 2016). The paleolatitude of the Baoshan area is ~20–24°N (Huang & Opdyke, 1993 and this study). If the paleolatitude from the Yanshiping area is removed because of possible inclination shallowing, the other data would suggest a 6–10° (~700–1,000 km) paleolatitude difference between the Gaize and Baoshan, which also indicates a ~N60°W trend of Qiangtang from west to east (Figure 11), consistent with the result from paleomagnetic declinations.

6. Conclusions

We reported a new paleomagnetic study on the Middle Jurassic and Paleocene rocks in Baoshan, northern Sibumasu. Rock magnetic studies indicate that hematite is the main remanence carrier. The primary character of the characteristic remanent magnetization of the Middle Jurassic and Paleocene rocks is supported by a detrital origin of the hematite as indicated by SEM results, a positive regional fold test and reversal test. The tilt-corrected mean direction of the Middle Jurassic Luzijing Formation ($\text{Dec} \pm \Delta D_x = 79.5 \pm 2.2^\circ$, $\text{Inc} \pm \Delta I_x = 39.3 \pm 2.0^\circ$, $n = 71$, $K = 66.9$, $A_{95} = 2.1^\circ$, $A_{95\text{min,max}} = [2.2, 5.6]$) and of the Paleocene Muguahé Formation ($\text{Dec} \pm \Delta D_x = 72.5 \pm 3.3^\circ$, $\text{Inc} \pm \Delta I_x = 10.0 \pm 6.5^\circ$, $n = 139$, $K = 14$, $A_{95} = 3.3^\circ$, $A_{95\text{min,max}} = [1.7, 3.7]$) imply a significantly large (~70–80°) clockwise rotation of Baoshan area since Paleocene. This result, in combination with previous published results, suggests that the northern Sibumasu region, cut by a series of NE–SW strike-slip faults, experienced a much larger clockwise rotation than the remaining areas of southeast margin of Tibetan Plateau. We ascribe this large rotation by a sum of rotation in the early Cenozoic associated with Indochina extrusion and rotation after the middle Miocene associated with the southeastward extrusion of Tibetan crust along the Xianshuihe–Xiaojiang fault. If correct, this indicates that the eastward motion of Tibetan crust crossed the Ailao Shan–Red River fault and transferred through the southwestern Yunnan toward Myanmar. Our paleomagnetic results, together with Jurassic/Cretaceous paleomagnetic data from Qiangtang/Sibumasu, suggest that the Qiangtang/northern Sibumasu changed from a precollisional strike of ~N60°W in eastern Tibet to N10°W in southern Sibumasu.

Acknowledgments

S. Li and C. Deng acknowledge the financial support from the National Natural Science Foundation of China grant 41404056 and the State Key Laboratory of Lithospheric Evolution grant 11431780. E.L.A. and D.J.J.v.H. were funded through ERC starting grant 306810 (SINK). D.J.J.v.H. acknowledges NWO Vidi grant 864.11.004. We thank Wenbin Wu for laboratory assistance. All the data for this paper have been uploaded in the supporting information table.

References

- Akciz, S., Burchfiel, B. C., Crowley, J. L., Yin, J., & Chen, L. (2008). Geometry, kinematics, and regional significance of the Chong Shan shear zone, Eastern Himalayan syntaxis, Yunnan, China. *Geoscience*, *4*, 292–314. <https://doi.org/10.1130/GES00111.1>
- Bertrand, G., Rangin, C., Maluski, H., & Bellon, H. (2001). Diachronous cooling along the Mogok Metamorphic Belt (Shan scarp, Myanmar): The trace of the northward migration of the Indian syntaxis. *Journal of Asian Earth Sciences*, *19*(5), 649–659. [https://doi.org/10.1016/S1367-9120\(00\)00061-4](https://doi.org/10.1016/S1367-9120(00)00061-4)
- Biggin, A. J., Strik, G., & Langereis, C. G. (2008). Evidence for a very-long-term trend in geomagnetic secular variation. *Nature Geoscience*, *1*, 395–398.
- Blisniuk, P., Hacker, B. R., Glodny, J., Ratschbacher, L., Bi, S. W., Wu, Z. H., et al. (2001). Normal faulting in central Tibet since at least 13.5 Myr ago. *Nature*, *412*(6847), 628–632. <https://doi.org/10.1038/35088045>
- Burchfiel, B., Studnicki-Gizbert, C., Geissman, J., King, R., Chen, Z., Chen, L., & Wang, E. (Eds.) (2007). How much strain can continental crust accommodate without developing obvious through-going faults? *Geological Society of America Special Papers* (Vol. 433, pp. 51–61). [https://doi.org/10.1130/2007.2433\(03\)](https://doi.org/10.1130/2007.2433(03))
- Butler, R. (1992). *Paleomagnetism: Magnetic Domains to Geologic Terranes*, (p. 238). Boston, Massachusetts: Blackwell Scientific Publishing.
- Chen, W., Zhang, S., Ding, J., Zhang, J., Zhao, X., Zhu, L., et al. (2017). Combined paleomagnetic and geochronological study on Cretaceous strata of the Qiangtang terrane, central Tibet. *Gondwana Research*, *41*, 373–389. <https://doi.org/10.1016/j.gr.2015.07.004>
- Chung, S. L., Lee, T. Y., Lo, C. H., Wang, P. L., Chen, C. Y., Yem, N. T., et al. (1997). Intraplate extension prior to continental extrusion along the Ailao Shan Red River shear zone. *Geology*, *25*(4), 311–314.
- Clark, M., & Royden, L. H. (2000). Topographic ooze: Building the eastern margin of Tibet by lower crustal flow. *Geology*, *28*(8), 703–706. [https://doi.org/10.1130/0091-7613\(2000\)28%3C703:TOBTEM%3E2.0.CO;2](https://doi.org/10.1130/0091-7613(2000)28%3C703:TOBTEM%3E2.0.CO;2)
- Curry, J. R. (2005). Tectonics and history of the Andaman Sea region. *Journal of Asian Earth Sciences*, *25*(1), 187–232.
- Deenen, M., Langereis, C. G., van Hinsbergen, D. J. J., & Biggin, A. J. (2011). Geomagnetic secular variation and the statistics of palaeomagnetic directions. *Geophysical Journal International*, *186*(2), 509–520. <https://doi.org/10.1111/j.1365-246X.2011.05050.x>
- Fisher, R. (1953). Dispersion on a sphere. *Proceedings of the Royal Society of London, Series A*, *217*(1130), 295–305. <https://doi.org/10.1098/rspa.1953.0064>

- Fujiwara, K. P., Zaman, H., Surinkum, A., Chaiwong, N., Fujihara, M., Ahn, H.-S., & Otofujii, Y.-i. (2014). New insights into regional tectonics of the Indochina Peninsula inferred from Lower-Middle Jurassic paleomagnetic data of the Sibumasu Terrane. *Journal of Asian Earth Sciences*, *94*, 126–138. <https://doi.org/10.1016/j.jseas.2014.08.020>
- Fyhn, M., Boldreel, L. O., & Nielsen, L. H. (2009). Geological development of the Central and South Vietnamese margin: Implications for the establishment of the South China Sea, Indochinese escape tectonics and Cenozoic volcanism. *Tectonophysics*, *478*, 184–214. <https://doi.org/10.1016/j.tecto.2009.08.002>
- Gahalaut, V. K., Kundu, B., Laishram, S. S., Catherine, J., Kumar, A., Singh, M. D., et al. (2013). Aseismic plate boundary in the Indo-Burmese wedge, northwest Sunda Arc. *Geology*, *41*(2), 235–238. <https://doi.org/10.1130/G33771.1>
- Gao, L., Yang, Z., Tong, Y., Wang, H., & An, C. (2015). New paleomagnetic studies of Cretaceous and Miocene rocks from Jinggu, western Yunnan, China: Evidence for internal deformation of the Lanping–Simao Terrane. *Journal of Geodynamics*, *89*, 39–59. <https://doi.org/10.1016/j.jog.2015.06.004>
- Gao, L., Yang, Z., Tong, Y., Wang, H., An, C., & Zhang, H. (2017). New paleomagnetic results from the Chuan Dian Fragment (South China) and their tectonic implications. *Journal of Geodynamics*, *112*, 46–57.
- Gilley, L. (2003). Direct dating of left-lateral deformation along the Red River shear zone, China and Vietnam. *Journal of Geophysical Research*, *108*(B2), 2127. <https://doi.org/10.1029/2001JB001726>
- Hall, R. (2002). Cenozoic geological and plate tectonic evolution of SE Asia and the SW Pacific: Computer-based reconstructions, model and animations. *Journal of Asian Earth Sciences*, *20*(4), 353–431.
- Huang, K. N., & Opdyke, N. D. (1993). Paleomagnetic results from Cretaceous and Jurassic rocks of South and Southwest Yunnan: Evidence for large clockwise rotations in the Indochina and Shan–Thai–Malay terranes. *Earth and Planetary Science Letters*, *117*(3–4), 507–524. [https://doi.org/10.1016/0012-821x\(93\)90100-n](https://doi.org/10.1016/0012-821x(93)90100-n)
- Huang, K., Opdyke, N. D., Li, J. G., & Peng, X. J. (1992). Paleomagnetism of Cretaceous Rocks from Eastern Qiangtang terrane of Tibet. *Journal of Geophysical Research*, *97*(B2), 1789–1799. <https://doi.org/10.1029/91JB02747>
- Johnson, C. L., Constable, C. G., Tauxe, L., Barendregt, R., Brown, L. L., Coe, R. S., et al. (2008). Recent investigations of the 0–5 Ma geomagnetic field recorded by lava flows. *Geochemistry, Geophysics, Geosystems*, *9*, Q04032. <https://doi.org/10.1029/2007GC001696>
- Kirby, E., Reiners, P. W., Krol, M. A., Whipple, K. X., Hodges, K. V., Farley, K. A., et al. (2002). Late Cenozoic evolution of the eastern margin of the Tibetan Plateau: Inferences from $^{40}\text{Ar}/^{39}\text{Ar}$ and (U–Th)/He thermochronology. *Tectonics*, *21*(1), 1001. <https://doi.org/10.1029/2000TC001246>
- Kirschvink, J. (1980). The least-squares line and plane and the analysis of palaeomagnetic data. *Geophysical Journal International*, *62*(3), 699–718. <https://doi.org/10.1111/j.1365-246X.1980.tb02601.x>
- Kornfeld, D., Eckert, S., Appel, E., Ratschbacher, L., Pfänder, J., Liu, D., & Ding, L. (2014). Clockwise rotation of the Baoshan Block due to southeastward tectonic escape of Tibetan crust since the Oligocene. *Geophysical Journal International*, *197*(1), 149–163. <https://doi.org/10.1093/gji/ggu009>
- Kornfeld, D., Eckert, S., Appel, E., Ratschbacher, L., Sonntag, B. L., Pfänder, J. A., et al. (2014). Cenozoic clockwise rotation of the Tengchong block, southeastern Tibetan Plateau: A paleomagnetic and geochronologic study. *Tectonophysics*, *628*, 105–122. <https://doi.org/10.1016/j.tecto.2014.04.032>
- Kornfeld, D., Sonntag, B.-L., Gast, S., Matthes, J., Ratschbacher, L., Pfänder, J. A., et al. (2014). Apparent paleomagnetic rotations reveal Pliocene–Holocene internal deformation of the Tengchong Block, southeastern Tibetan Plateau. *Journal of Asian Earth Sciences*, *96*(0), 1–16. <https://doi.org/10.1016/j.jseas.2014.08.034>
- Koymans, M. R., Langereis, C. G., Pastor-Galán, D., & van Hinsbergen, D. J. J. (2016). Paleomagnetism.org: An online multi-platform open source environment for paleomagnetic data analysis. *Computational Geosciences*, *93*, 127–137. <https://doi.org/10.1016/j.cageo.2016.05.007>
- Kruiver, P. P., Dekkers, M. J., & Heslop, D. (2001). Quantification of magnetic coercivity components by the analysis of acquisition curves of isothermal remanent magnetisation. *Earth and Planetary Science Letters*, *189*(3–4), 269–276.
- Lacassin, R., Replumaz, A., & Leloup, P. H. (1998). Hairpin river loops and slip-sense inversion on southeast Asian strike-slip faults. *Geology*, *26*(8), 703–706.
- Leloup, P., Harrison, T. M., Ryerson, F., Wenji, C., Qi, L., Tapponnier, P., & Lacassin, R. (1993). Structural, petrological and thermal evolution of a Tertiary ductile strike-slip shear zone, Diancang Shan, Yunnan. *Journal of Geophysical Research*, *98*(B4), 6715–6743. <https://doi.org/10.1029/92JB02791>
- Leloup, P., Lacassin, R., Tapponnier, P., Schärer, U., Zhong, D. L., Liu, X. H., et al. (1995). The Ailao Shan–Red River shear zone (Yunnan, China), Tertiary transform boundary of Indochina. *Tectonophysics*, *251*(1–4), 3–84. [https://doi.org/10.1016/0040-1951\(95\)00070-4](https://doi.org/10.1016/0040-1951(95)00070-4)
- Leloup, P., Lacassin, R., Tapponnier, P., & Harrison, T. M. (2001). Comment on “Onset timing of left-lateral movement along the Ailao Shan–Red River shear zone: Ar-40/Ar-39 dating constraint from the Nam Dinh area, northeastern Vietnam” by Wang et al., 2000. *J. Asian Earth Sci.* *18*, 281–292 – Discussion. *Journal of Asian Earth Sciences*, *20*(1), 95–99.
- Li, S. H., Deng, C. L., Yao, H. T., Huang, S., Liu, C. Y., He, H. Y., et al. (2013). Magnetostratigraphy of the Dali Basin in Yunnan and implications for late Neogene rotation of the southeast margin of the Tibetan Plateau. *Journal of Geophysical Research: Solid Earth*, *118*, 791–807. <https://doi.org/10.1002/jgrb.50129>
- Li, S. H., Deng, C. L., Dong, W., Sun, L., Liu, S. Z., Qin, H. F., et al. (2015). Magnetostratigraphy of the Xiaolongtan Formation bearing *Lufengpithecus keiyuanensis* in Yunnan, southwestern China: Constraint on the initiation time of the southern segment of the Xianshuihe–Xiaojiang fault. *Tectonophysics*, *655*, 213–226. <https://doi.org/10.1016/j.tecto.2015.06.002>
- Li, Z., Ding, L., Lippert, P. C., Song, P., Yue, Y., & van Hinsbergen, D. J. J. (2016). Paleomagnetic constraints on the Mesozoic drift of the Lhasa terrane (Tibet) from Gondwana to Eurasia. *Geology*, *44*(9), 727–730. <https://doi.org/10.1130/g38030.1>
- Li, S., Yang, Z., Deng, C., He, H., Qin, H., Sun, L., et al. (2017). Clockwise rotations recorded in redbeds from the Jinggu Basin of northwestern Indochina. *Geological Society of America Bulletin*, *129*, 1100–1122. <https://doi.org/10.1130/b31637.1>
- Li, S., Advokaat, E. L., van Hinsbergen, D. J. J., Koymans, M., Deng, C., & Zhu, R. (2017). Paleomagnetic constraints on the Mesozoic–Cenozoic paleolatitudinal and rotational history of Indochina and South China: Review and updated kinematic reconstruction. *Earth Science Reviews*, *171*, 58–77. <https://doi.org/10.1016/j.earscirev.2017.05.007>
- Liu, C.-Z., Chung, S.-L., Wu, F.-Y., Zhang, C., Xu, Y., Wang, J.-G., et al. (2016). Tethyan suturing in Southeast Asia: Zircon U–Pb and Hf–O isotopic constraints from Myanmar ophiolites. *Geology*, *44*(4), 311–314. <https://doi.org/10.1130/g37342.1>
- Lowrie, W. (1990). Identification of ferromagnetic minerals in a rock by coercivity and unblocking temperature properties. *Geophysical Research Letters*, *17*(2), 159–162. <https://doi.org/10.1029/GL017i002p00159>
- Maurin, T., & Rangin, C. (2009). Structure and kinematics of the Indo-Burmese Wedge: Recent and fast growth of the outer wedge. *Tectonics*, *28*, TC2010. <https://doi.org/10.1029/2008TC002276>
- Mazur, S., Green, C., Stewart, M. G., Whittaker, J. M., Williams, S., & Bouatmani, R. (2012). Displacement along the Red River Fault constrained by extension estimates and plate reconstructions. *Tectonics*, *31*, TC5008. <https://doi.org/10.1029/2012TC003174>

- McFadden, P., & McElhinny, M. (1988). The combined analysis of remagnetization circles and direct observations in palaeomagnetism. *Earth and Planetary Science Letters*, *87*, 161–172.
- McFadden, P., & McElhinny, M. (1990). Classification of the reversal test in palaeomagnetism. *Geophysical Journal International*, *103*(3), 725–729. <https://doi.org/10.1111/j.1365-246X.1990.tb05683.x>
- Metcalfe, I. (1996). Gondwanaland dispersion, Asian accretion and evolution of eastern Tethys. *Australian Journal of Earth Sciences*, *43*(6), 605–623. <https://doi.org/10.1080/08120099608728282>
- Metcalfe, I. (2013). Gondwana dispersion and Asian accretion: Tectonic and palaeogeographic evolution of eastern Tethys. *Journal of Asian Earth Sciences*, *66*, 1–33. <https://doi.org/10.1016/j.jseas.2012.12.020>
- Mitchell, A. H. G., Htay, M. T., & Htun, K. M. (2015). The medial Myanmar suture zone and the western Myanmar-Mogok foreland. *Myanmar Geological Society of Japan*, *6*, 73–88.
- Otofuji, Y., Inoue, Y., Funahara, S., Murata, F., & Zheng, X. (1990). Palaeomagnetic study of eastern Tibet—deformation of the Three Rivers region. *Geophysical Journal International*, *103*(1), 85–94. <https://doi.org/10.1111/j.1365-246X.1990.tb01754.x>
- Replumaz, A., Karason, H., van der Hilst, R. D., Besse, J., & Tapponnier, P. (2004). 4-D evolution of SE Asia's mantle from geological reconstructions and seismic tomography. *Earth and Planetary Science Letters*, *221*(1–4), 103–115.
- Replumaz, A., Negredo, A. M., Guillot, S., der Beek, P. V., & Villaseñor, A. (2010). Crustal mass budget and recycling during the India/Asia collision. *Tectonophysics*, *492*(1–4), 99–107. <https://doi.org/10.1016/j.tecto.2010.05.023>
- Roberts, A., Cui, Y. L., & Verosub, K. L. (1995). Wasp-waisted hysteresis loops: Mineral magnetic characteristics and discrimination of components in mixed magnetic systems. *Journal of Geophysical Research*, *100*(B9), 17,909–17,924. <https://doi.org/10.1029/95JB00672>
- Roger, F., Calassou, S., Lancelot, J., Malavieille, J., Mattauer, M., Xu, Z. Q., et al. (1995). Miocene emplacement and deformation of the Konga-Shan granite (Xianshui-He Fault Zone, West Sichuan, China) – Geodynamic Implications. *Earth and Planetary Science Letters*, *130*(1–4), 201–216. [https://doi.org/10.1016/0012-821X\(94\)00252-T](https://doi.org/10.1016/0012-821X(94)00252-T)
- Royden, L. H., Burchfiel, B. C., & van der Hilst, R. D. (2008). The geological evolution of the Tibetan Plateau. *Science*, *321*(5892), 1054–1058. <https://doi.org/10.1126/science.1155371>
- Schoenbohm, L., Burchfiel, B. C., Chen, L., & Yin, J. (2006). Miocene to present activity along the Red River fault, China, in the context of continental extrusion, upper-crustal rotation, and lower-crustal flow. *Geological Society of America Bulletin*, *118*(5–6), 672–688. <https://doi.org/10.1130/B25816.1>
- Schoenbohm, L., Burchfiel, B. C., & Chen, L. Z. (2006). Propagation of surface uplift, lower crustal flow, and Cenozoic tectonics of the southeast margin of the Tibetan Plateau. *Geology*, *34*(10), 813–816. <https://doi.org/10.1130/G22679.1>
- Searle, M. P., Noble, S. R., Cottle, J. M., Waters, D. J., Mitchell, A. H. G., Hlaing, T., & Horstwood, M. S. A. (2007). Tectonic evolution of the Mogok metamorphic belt, Burma (Myanmar) constrained by U-Th-Pb dating of metamorphic and magmatic rocks. *Tectonics*, *26*, TC3014. <https://doi.org/10.1029/2006TC002083>
- Searle, M., Yeh, M. W., Lin, T. H., & Chung, S. L. (2010). Structural constraints on the timing of left-lateral shear along the Red River shear zone in the Ailao Shan and Diancang Shan Ranges, Yunnan, SW China. *Geoscience*, *6*(4), 316–338. <https://doi.org/10.1130/GES00580.1>
- Sevastjanova, I., Hall, R., Rittner, M., Paw, S. M. T. L., Naing, T. T., Alderton, D. H., & Comfort, G. (2016). Myanmar and Asia united, Australia left behind long ago. *Gondwana Research*, *32*, 24–40. <https://doi.org/10.1016/j.gr.2015.02.001>
- Socquet, A., & Pubellier, M. (2005). Cenozoic deformation in western Yunnan (China–Myanmar border). *Journal of Asian Earth Sciences*, *24*(4), 495–515. <https://doi.org/10.1016/j.jseas.2004.03.006>
- Song, P., Ding, L., Li, Z., Lippert, P. C., & Yue, Y. (2017). An early bird from Gondwana: Paleomagnetism of Lower Permian lavas from northern Qiangtang (Tibet) and the geography of the Paleo-Tethys. *Earth and Planetary Science Letters*, *475*, 119–133. <https://doi.org/10.1016/j.epsl.2017.07.023>
- Tapponnier, P., Peltzer, G., Le Dain, A. Y., Armijo, R., & Cobbold, P. (1982). Propagating extrusion tectonics in Asia: New insights from simple experiments with plasticine. *Geology*, *10*(12), 611–616. [https://doi.org/10.1130/0091-7613\(1982\)10%3C611:petian%3E2.0.co;2](https://doi.org/10.1130/0091-7613(1982)10%3C611:petian%3E2.0.co;2)
- Tauxe, L. (2010). *Essentials of Paleomagnetism* (p. 512). Berkeley, CA: University of California Press.
- Tauxe, L., & Watson, G. S. (1994). The fold test: An eigen analysis approach. *Earth and Planetary Science Letters*, *122*(3), 331–341. [https://doi.org/10.1016/0012-821X\(94\)90006-X](https://doi.org/10.1016/0012-821X(94)90006-X)
- Tong, Y.-B., Yang, Z., Gao, L., Wang, H., Zhang, X.-D., An, C.-Z., et al. (2015). Paleomagnetism of Upper Cretaceous red-beds from the eastern Qiangtang Block: Clockwise rotations and latitudinal translation during the India–Asia collision. *Journal of Asian Earth Sciences*, *114*, 732–749. <https://doi.org/10.1016/j.jseas.2015.08.016>
- Tong, Y., Yang, Z., Jing, X., Zhao, Y., Li, C., Huang, D., & Zhang, X. (2016). New insights into the Cenozoic lateral extrusion of crustal blocks on the southeastern edge of Tibetan Plateau: Evidence from paleomagnetic results from Paleogene sedimentary strata of the Baoshan Terrane. *Tectonics*, *35*, 2494–2514. <https://doi.org/10.1002/2016TC004221>
- Torsvik, T. H., van der Voo, R., Preeden, U., Mac Niocaill, C., Steinberger, B., Doubrovine, P. V., et al. (2012). Phanerozoic polar wander, paleogeography and dynamics. *Earth Science Reviews*, *114*(3–4), 325–368. <https://doi.org/10.1016/j.earscirev.2012.06.007>
- van Hinsbergen, D. J. J., Kapp, P., Dupont-Nivet, G., Lippert, P. C., DeCelles, P. G., & Torsvik, T. H. (2011). Restoration of Cenozoic deformation in Asia and the size of Greater India. *Tectonics*, *30*, TC5003. <https://doi.org/10.1029/2011TC002908>
- Wang, E., & Burchfiel, B. C. (1997). Interpretation of Cenozoic tectonics in the right-lateral accommodation zone between the Ailao Shan shear zone and the eastern Himalayan syntaxis. *International Geology Review*, *39*(3), 191–219. <https://doi.org/10.1080/00206819709465267>
- Wang, E., Burchfiel, B. C., Royden, L. H., Chen, L. Z., Chen, J. S., Li, W. X., & Chen, Z. L. (1998). Late Cenozoic Xianshuihe-Xiaojiang, Red River, and Dali fault systems of southwestern Sichuan and Central Yunnan, China. *Geological Society of America Special Papers*, *327*, 1–108. <https://doi.org/10.1130/0%2E2%80%9338137%E2%80%9332327-2.1>
- Wang, X., Metcalfe, I., Jian, P., He, L., & Wang, C. (2000). The Jinshajiang–Ailaoshan suture zone, China: Tectonostratigraphy, age and evolution. *Journal of Asian Earth Sciences*, *18*, 675–690.
- Wang, Y., Fan, W., Zhang, Y., Peng, T., Chen, X., & Xu, Y. (2006). Kinematics and $^{40}\text{Ar}/^{39}\text{Ar}$ geochronology of the Gaoligong and Chongshan shear systems, western Yunnan, China: Implications for early Oligocene tectonic extrusion of SE Asia. *Tectonophysics*, *418*(3), 235–254. <https://doi.org/10.1016/j.tecto.2006.02.005>
- Wang, S., Fang, X. M., Zheng, D. W., & Wang, E. C. (2009). Initiation of slip along the Xianshuihe fault zone, eastern Tibet, constrained by K/Ar and fission-track ages. *International Geology Review*, *51*(12), 1121–1131. <https://doi.org/10.1080/00206810902945132>
- Wang, Y., Sieh, K., Tun, S. T., Lai, K.-Y., & Myint, T. (2014). Active tectonics and earthquake potential of the Myanmar region. *Journal of Geophysical Research*, *119*, 3767–3822. <https://doi.org/10.1002/2013JB010762>
- Yan, M., Zhang, D., Fang, X., Ren, H., Zhang, W., Zan, J., et al. (2016). Paleomagnetic data bearing on the Mesozoic deformation of the Qiangtang Block: Implications for the evolution of the Paleo- and Meso-Tethys. *Gondwana Research*, *39*, 292–316. <https://doi.org/10.1016/j.gr.2016.01.012>

- Yang, Z. Y., Besse, J., Suteethorn, V., Bassoullet, J. P., Fontaine, H., & Buffetaut, E. (1995). Lower-Middle Jurassic paleomagnetic data from the Mae Sot area (Thailand): Paleogeographic evolution and deformation history of southeastern Asia. *Earth and Planetary Science Letters*, *136*(3–4), 325–341. [https://doi.org/10.1016/0012-821X\(95\)00192-F](https://doi.org/10.1016/0012-821X(95)00192-F)
- Yang, Z. Y., Yin, J. Y., Sun, Z. M., Otofujii, Y., & Sato, K. (2001). Discrepant Cretaceous paleomagnetic poles between Eastern China and Indochina: A consequence of the extrusion of Indochina. *Tectonophysics*, *334*(2), 101–113. [https://doi.org/10.1016/S0040-1951\(01\)00061-0](https://doi.org/10.1016/S0040-1951(01)00061-0)
- Yunnan Bureau of Geology and Mineral Resources (YBGMR) (1990). *Regional Geology of Yunnan Province* (pp. 1–726). Beijing: Geological Publishing House. (In Chinese)
- Zhai, Q. G., Jahn, B. M., Wang, J., Su, L., Mo, X. X., Wang, K. L., et al. (2013). The Carboniferous ophiolite in the middle of the Qiangtang terrane, northern Tibet: SHRIMP U–Pb dating, geochemical and Sr–Nd–Hf isotopic characteristics. *Lithos*, *168–169*, 186–199. <https://doi.org/10.1016/j.lithos.2013.02.005>
- Zhang, P., Shen, Z., Wang, M., Gan, W. J., Burgmann, R., & Molnar, P. (2004). Continuous deformation of the Tibetan Plateau from global positioning system data. *Geology*, *32*(9), 809–812. <https://doi.org/10.1130/G20554.1>
- Zhang, B., Zhang, J. J., Zhong, D. L., Yang, L. K., Yue, Y. H., & Yan, S. Y. (2012). Polystage deformation of the Gaoligong metamorphic zone: Structures, Ar–40/Ar–39 mica ages, and tectonic implications. *Journal of Structural Geology*, *37*, 1–18. <https://doi.org/10.1016/j.jsg.2012.02.007>
- Zhu, R., Potts, R., Pan, Y. X., Lue, L. Q., Yao, H. T., Deng, C. L., & Qin, H. F. (2008). Paleomagnetism of the Yuanmou Basin near the southeastern margin of the Tibetan Plateau and its constraints on late Neogene sedimentation and tectonic rotation. *Earth and Planetary Science Letters*, *272*, 97–104. <https://doi.org/10.1016/j.epsl.2008.04.016>